



### **Science Arts & Métiers (SAM)**

is an open access repository that collects the work of Arts et Métiers Institute of Technology researchers and makes it freely available over the web where possible.

This is an author-deposited version published in: <https://sam.ensam.eu>  
Handle ID: <http://hdl.handle.net/10985/19661>

#### **To cite this version :**

Jinyang XU, Ming CHEN, Fei REN, Mohamed EL MANSORI - Orthogonal cutting mechanisms of CFRP/Ti6Al4V stacks - International Journal of Advanced Manufacturing Technology - Vol. 103, n°9-12, p.3831-3851 - 2019

Any correspondence concerning this service should be sent to the repository

Administrator : [scienceouverte@ensam.eu](mailto:scienceouverte@ensam.eu)



# Orthogonal cutting mechanisms of CFRP/Ti6Al4V stacks

Jinyang Xu<sup>1</sup> · Mohamed El Mansori<sup>2,3</sup> · Ming Chen<sup>1</sup> · Fei Ren<sup>4</sup>

## Abstract

The enhanced mechanical/physical properties and improved functionalities have made the carbon fiber-reinforced polymer/titanium alloy (CFRP/Ti6Al4V) stacks very attractive to the modern aerospace industry. However, the current knowledge of machining CFRP/Ti6Al4V stacks remains insufficient to guide their industrial applications. The main contribution of the present paper lies in the scientific understanding of the coupling effects and underlying mechanisms dominating the stack chip formation and cutting response transfer via the orthogonal cutting method. A particular focus was placed on the identification of the impact of different cutting sequence strategies (i.e., cutting from CFRP to Ti6Al4V and from Ti6Al4V to CFRP) on the stack machinability. The orthogonal cutting tests were carefully performed on a shaper machine tool using the polycrystalline diamond (PCD)-tipped inserts. The present study covers a variety of aspects in the CFRP/Ti6Al4V machining including the chip removal process, cutting forces, chip features, bouncing-back phenomenon and machined surface quality. The results discussed in this work allow for a better cutting understanding of CFRP/Ti6Al4V stacks and could advance the state of knowledge of the subject area.

**Keywords** CFRP/Ti6Al4V stacks · Orthogonal cutting · Cutting mechanisms · Chip formation · Machined surface characteristics

## 1 Introduction

Within the last decade, there has been a trend of increasing demand of lightweight metallic-composite stacks in the aeronautical industry due to the need of developing advanced mechanical structures favoring the system improvement and the energy saving of the modern aircraft. Materials made of multilayers of carbon fiber-reinforced polymer (CFRP) composites and titanium (Ti) alloys are a typical example of compound stacks. These hybrid structures possess excellent mechanical properties like high specific strength/stiffness and excellent fatigue/corrosion resistance with a relatively low weight at

the same time, which makes them especially interesting for structural components in the aircraft industry or other high-tech applications [1, 2]. Moreover, the multilayer stacks are serving as a good alternative to conventional standard fibrous composites and single metal alloys in a variety of applications where both component weight and structural performance are critical concerns [3, 4]. Aircraft structures subjected to high thermo-mechanical stresses are successfully fabricated with these compound materials. The wing-fuselage connections of the Boeing 787 Dreamliner are a typical application [4].

Owing to the riveting and bolting purposes, mechanical drilling has been frequently used in the near-net shape processing of CFRP/Ti6Al4V stacks in order to meet dimensional tolerance, surface quality and other functional requirements. Because of the advantage in productivity, it is desirable for the CFRP/Ti6Al4V stacks to be drilled in one-shot pass with a single drill. The tolerance requirement on these holes is much higher than in many other industries due to safety reasons. Drilling holes in these dissimilar materials in a stack form with close tolerance is quite challenging because of the completely different cutting characteristics between two materials and the severe tool wear resulting in poor hole quality. For instance, fibrous composites are by nature inhomogeneous and highly abrasive, possessing poor machinability resulting in serious damage involving delamination, cracking, fiber pullouts, etc.

---

✉ Jinyang Xu  
xujinyang@sjtu.edu.cn

<sup>1</sup> State Key Laboratory of Mechanical System and Vibration, School of Mechanical Engineering, Shanghai Jiao Tong University, Shanghai 200240, People's Republic of China

<sup>2</sup> MSMP – EA 7350, Arts et Métiers ParisTech, 51006 Châlons-en-Champagne, France

<sup>3</sup> Department of Mechanical Engineering, Texas A&M University, College Station, TX 77840, USA

<sup>4</sup> Shanghai Aerospace Equipments Manufacturer Co., Ltd., Shanghai 200245, People's Republic of China

[5–9]; titanium alloys exhibit poor thermal conductivity, low elastic modulus, and high chemical affinity to most-used tool materials, machining of which entails high cutting forces, high cutting temperatures, and rapid tool wear. Additionally, the presence of the spatial discontinuities in the bi-material interface makes it difficult to define machining strategies that contemplate a small number of parameters affecting the functional performance. The aforementioned characteristics complicate the chip separation process and the defect formation mechanisms of the bi-material structure. The key challenges of drilling metallic-composite stacks are often manifested by serious geometrical imperfections, large extents of subsurface damage, and excessive tool wear as reported in refs. [10–15].

To date, a substantial number of experimental investigations [15–21] have been interested to deal with the machining of metallic-composite stacks, covering a variety of topics including drilling forces, parametric effects, hole quality, tool wear, etc. A review article published by Xu et al. reporting the key advances in drilling FRP/Ti stacks is available in [4]. Despite the fact that the extensive research results have been published concerning drilling CFRP/Ti6Al4V stacks, the drilling operation still remains rather difficult to inspect the fundamental mechanisms governing the chip separation process and the cutting response of the bi-material structure because of the complicated tool-chip interaction features and the inherent internal nature of drilling. In contrast, the orthogonal cutting configuration derived from various complex machining processes (e.g., drilling and milling) represents a handy method that could provide a more fundamental insight into the physical phenomena promoted in an actual manufacturing process of this sandwich material. In light of this advantage, the orthogonal cutting has been widely used to shed light on the underlying mechanisms in the chip removal processes of both fibrous composites and titanium alloys. One of the early representative studies utilizing the orthogonal cutting method for quantitative analyses of composite machining characteristics was performed by Koplev et al. [22] dating back to the early 1980s. The authors pointed out that the machining of CFRP composites entails a large number of tiny chips due to the dominant chip separation mode of brittle fracture. Following this preceding work, Wang et al. [23] and Arola et al. [24] conducted a series of orthogonal cutting tests on graphite/epoxy composites using polycrystalline diamond (PCD) tools. The chip separation modes of different fiber-oriented laminates were discussed in detail with respect to tool geometries and process parameters. The experimental results revealed several cutting mechanisms consisting of delamination, fiber buckling, fiber cutting, deformation, and shearing responsible for the discontinuous chip formation of fibrous composites. Additionally, the fiber orientation was noted as an influential factor in cutting forces and surface morphologies during the machining of graphite/epoxy composites. On the other hand, Pwu and Hocheng [25] developed

an analytical model to offer a deep insight into the chip formation of orthogonal cutting of FRP composites and found that the chip separation in thickness due to intrinsic bonding defects and overbent chips due to inhomogeneous local material strength predominate in the case of cutting fiber-reinforced plastics perpendicular to the fiber axis. Wang and Zhang [26] revealed that the bouncing back is a characteristic phenomenon associated with the cutting of FRPs and three distinct deformation zones appear involving chipping, pressing and bouncing when the fiber orientation is within  $90^\circ$ . Owing to the fiber-dependent machinability and anisotropic physical behavior, composite materials raise some specific problems during machining. Fibers used as reinforcement cause rapid abrasive wear in the form of cutting edge rounding and damage such as delamination, cracking, fiber splintering, or matrix thermal degradation are prevalent during the chip removal process, leading to a significant rejection rate of machined composite parts as stated by Brinksmeier et al. [27]. Apart from the mentioned experimental studies, numerical simulation and FE analysis of composite cutting physics using orthogonal cutting configuration have become a hot research topic in recent decades, providing in-depth inspections of the dynamic mechanisms governing the tool-chip and tool-work interactions during the material removal process [28–33]. Unlike fibrous composites, titanium alloys are isotropic in nature and exhibit elastoplastic behavior. These metallic materials are considered difficult to cut because of their low thermal conductivity, inherent high strength property maintained at elevated temperatures, and high tendency to form localized shear bands in machining. Machining titanium alloys involves serrated chip formation even at relatively low cutting speeds [34], causing high fluctuations of cutting forces acting over a very small tool-chip contact area (about one-third that in the case of steel) [35]. Previous studies have indicated two theories accounting for the basic origin of saw-tooth chips including the thermoplastic instability associated with the adiabatic shear bands [36–38] and the initiation and propagation of cracks inside the primary shear zone of the workpiece material [39, 40]. Further, high cutting forces, high localized temperatures at the tool-chip interface, thermally activated diffusion as well as chip adhesion at the cutting edges are the key characteristics when machining titanium alloys, resulting in the poor surface integrity, rapid tool wear, and short tool lifetime [2, 41].

Although the mechanisms of the orthogonal cutting of individual fibrous composites and titanium alloys have been extensively studied, the obtained knowledge cannot be fully applied to machining these two materials in a stack form since interrelated cutting phenomena predominate in the chip removal process. This is due to the fact that machining either the composite phase or the metallic phase first would exert several influences on the post-cut phase, primarily depending on the implemented cutting-sequence strategy. Such physical

phenomena are often manifested by the coupling tool wear and the impact of the chip evacuation of metals on the drilled composite surface. The above evidence has been widely noted for metallic-composite stacks particularly subjected to a drilling operation in the open literature [10, 11, 15, 16].

To understand the 3D drilling of CFRP/Ti6Al4V stacks, it requires to understand the fundamental behavior of one drill cutting edge when it moves from CFRP to titanium or vice versa. To select the cutting tool geometries based on the worst-case scenario, it is necessary to understand the cutting edge/material interactions using the selected configuration. Moreover, what in a metallic-composite stack could be done with a single tool in a single pass is taking three to five passes in a titanium and composite structure, i.e., drilling it multiple times and then running some forms of reamer with a counter-sink. The main objective of the present work is to address the mechanisms and strategies for composite/titanium stack drilling in one shot. The process can be represented, in the simplest terms, as force traveling on the surface of the stacked workpiece (independently of the way to bond the interface). This force changes in time and space so do its components, related to a reference frame attached to the workpiece. In the first fundamental level of the analysis, the goal is to establish the variability of all forces/quality responses as a function of cutting conditions such as cutting speed and depth of cut. The orthogonal cutting derived from the multilayer stack drilling was designed to shed light on the underlying mechanisms behind drilling. The present work was an extension of our previous investigations under the context of CFRP/Ti6Al4V stack orthogonal cutting [3, 42–46]. Two different cutting sequence strategies (CFRP  $\rightarrow$  Ti and Ti  $\rightarrow$  CFRP) that are frequently used in the stack drilling were considered. The CFRP/Ti6Al4V specimens were specifically customized in order to conform with the design of the stack orthogonal cutting. The in-situ chip separation process and varying force signatures in the function of cutting time were respectively recorded by a CCD camera and a Kistler dynamometer to facilitate the stack cutting comprehension. The post-process examinations include the studies of the resected chip features, and the morphologies and damage modes of the cut stack surfaces. The results discussed in this work qualify to create a better understanding that would assist in the process optimization and tool design when drilling CFRP/Ti6Al4V stacks.

## 2 Materials and methods

### 2.1 Workpiece and tool information

In this work, two difficult-to-cut materials of widespread use in the aeronautical industry have been investigated including carbon fiber-reinforced polymers (CFRP) and Ti6Al4V alloys. To conform with the design of the stack orthogonal

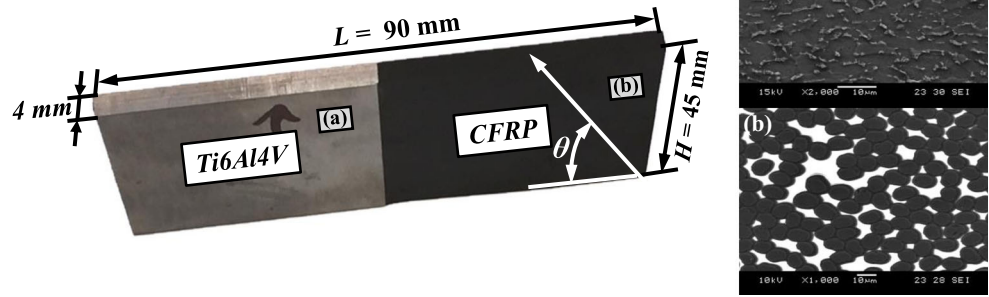
cutting, plates of unidirectional (UD) T300/914 carbon/epoxy composites and sheets of Ti6Al4V alloys were specifically customized. Both the constituents having an identical size of 4 mm (thickness)  $\times$  45 mm (length)  $\times$  45 mm (width) were bonded together using the 3-M Scotch-Weld™ 7240 FR B/A epoxy adhesive to create a firmly connected interface. A photograph showing the overall dimensions and microstructures of the utilized CFRP/Ti6Al4V stacks is given in Fig. 1. The Ti6Al4V is a most-used alpha-beta ( $\alpha + \beta$ ) titanium alloy containing a duplex microstructure with roughly 60% of primary  $\alpha$  nodules  $\alpha_p$  phase and 40% of lamellar colonies of second  $\alpha$  and  $\beta$  phases ( $\alpha_s + \beta$ ), while the T300/914 laminate is a polymer matrix composite reinforced by highly abrasive carbon fibers with an average diameter of 7  $\mu$ m. Each multilayer stack includes one Ti6Al4V sheet and one UD-CFRP laminate with a fiber orientation ( $\theta$ ) of either 0°, 45°, or 90°.

To finalize the orthogonal cutting tests, the polycrystalline diamond (PCD)-tipped tools prepared by brazing the commercially available CD10-grade PCD onto tungsten carbide inserts were adopted. The inserts were triangular in shape composed of fine to medium-fine grain crystals with an average diameter of 7  $\mu$ m, which were provided by Sandvik Coromant. The cutting edge has a rake angle ( $\alpha$ ) of 0°, a clearance angle ( $\gamma$ ) of 7°, and an effective cutting length of 7.4 mm. The cutting tools used were the same as those utilized in our previous studies [3, 45] where the tool geometrical details can be found.

### 2.2 Orthogonal cutting tests

The orthogonal cutting configuration was derived from the stack drilling process to achieve an easy inspection of the underlying mechanisms and strategies of the multi-material system despite an oblique cutting being more analogous to the drilling operation. The orthogonal machining experiments were conducted on a GSP-EL 136 shaper. The CFRP/Ti6Al4V stack was rigidly clamped with 3–5 mm of the specimen exposed between two hard steel plates inside a fixture mounted on a piezoelectric Kistler dynamometer. To conform with the industrial manufacturing conditions as well as increase productivity, each hole of the CFRP/Ti6Al4V stack was drilled in one-shot time using a single drill bit. The Kistler dynamometer (model 9255B) was firmly clamped on the shaper table and connected with a multichannel charge amplifier (model 5019 B131), an A/D board and a PC in order to acquire the force signals generated in the chip removal process. A LabVIEW program was employed to collect the data at an acquisition frequency of 1000 Hz. A charge-coupled device (FASTCAM SA5 CCD Camera) with a microscope lens and a strobed copper-vapor laser illumination system was utilized for recording optical frames to allow a direct observation of the chip formation zone at an acquisition rate of 20,000 frames/s. The camera lens was placed exactly in

**Fig. 1** A photograph showing one typical CFRP/Ti6Al4V stack. **a** The microstructure of the Ti6Al4V alloy. **b** The microstructure of the UD-CFRP composite



front of the side face of the metallic-composite stack with a particular focus on the interface region. Figure 2 provides a schematic illustration of the experimental setup for the orthogonal cutting of CFRP/Ti6Al4V stacks. The cutting tests were performed by varying the fiber cutting angle, the cutting speed, and the depth of cut, and the detailed cutting conditions are listed in Table 1. A full factorial design of experiments was used in order to analyze carefully the effects of the cutting parameters on the stack machinability. Two different cutting-sequence strategies, i.e., cutting from CFRP to Ti and from Ti to CFRP were implemented throughout the experiments. The machining tests were performed under dry cutting conditions to conform with most industrial specifications.

After the completion of the orthogonal cutting tests, the post-process analyses were conducted on the resected chips and the machined stack surfaces. Both composite and titanium chips generated from different cutting conditions were gathered to study their geometries and morphologies. The composite chips were characterized using a Nikon toolmaker's microscope. Free and back surfaces of titanium chips were examined using a JEOL JSM-5510 LV scanning electron microscope (SEM). To quantify their segmentation features, the titanium chips mounted in cold resin were ground, polished, and subsequently etched with 4% Nital (96–98 mL ethanol and 2–4 mL nitric acid ( $\text{HNO}_3$ )) for 2–5 s at room temperature. Afterward, an image analysis software built in the optical microscope was used to measure the geometrical parameters of the chip cross section. To improve the imaging quality, the

machined CFRP/Ti6Al4V surfaces were firstly cleaned using an ultrasonic cleaning device and finally characterized using both optical microscope and SEM. The most-used surface roughness parameter—arithmetic mean roughness ( $R_a$ )—was adopted to quantify the machined stack surface finish utilizing a Veeco interferometer, and the obtained results were correlated with the formation of chips and the input cutting parameters.

### 3 Results and discussion

#### 3.1 Characteristics of CFRP/Ti6Al4V cutting process

Machining metallic-composite stacks involves complicated physical phenomena associated with the chip removal process due to the multi-tool-work interaction domain. To inspect the characteristics of the bi-material cutting operation, force signals promoted in the cutting process were recorded. Specifically, the force signatures of the stack orthogonal cutting were decomposed into two basic components, i.e., cutting force ( $F_c$ ) and thrust force ( $F_t$ ), which respectively signify the in-situ status of the tool-chip interaction and the tool-work interaction during the material removal. Fig. 3 shows the obtained results with respect to different fiber orientations and cutting-sequence strategies under the fixed conditions of  $v_c = 80$  m/min and  $a_p = 0.20$  mm. It is noticeable that the force profiles generated in either  $0^\circ$  or  $45^\circ$  CFRP/Ti6Al4V stacks

**Fig. 2** A schematic diagram of the experimental setup for the orthogonal cutting of CFRP/Ti6Al4V stacks

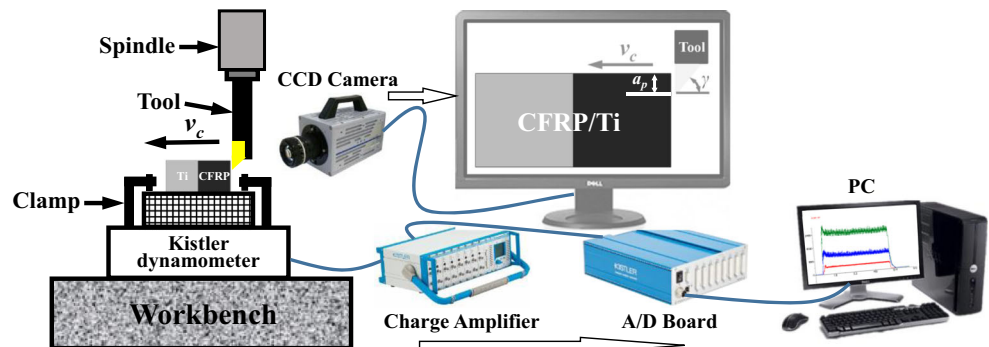


**Table 1** Cutting conditions for the orthogonal cutting of CFRP/Ti6Al4V stacks

Titanium alloy	Ti6Al4V
CFRP composite	T300/914 carbon/epoxy
Fiber volume fraction	60%
Fiber orientation ( $\theta$ )	0°, 45°, 90°, 135°
Tipped material of inserts	Polycrystalline diamond (PCD)
Tool substrate	Tungsten carbide
Effective cutting length	7.4 mm
Tool rake angle ( $\alpha$ )	0°
Tool clearance angle ( $\gamma$ )	7°
Cutting speed ( $v_c$ )	20, 32, 50, 80 m/min
Cutting width ( $a_w$ )	4 mm
Depth of cut ( $a_p$ )	0.05, 0.10, 0.15, 0.20 mm
Cutting length per step	90 mm
Cutting environment	Dry conditions

exhibit a similar variation trend with the cutting time. The phenomenon suggests a process of five cutting stages characterizing the in-situ status of the tool-chip interaction in the entire stack machining operation. The first and the last stages respectively denote the cut-in and cut-off processes of the stack where a rapid increase or decrease of force signatures is identified. In contrast, the second and the fourth stages suggest a full tool edge engagement in cutting either the fibrous composite or the titanium alloy depending on the utilized cutting-sequence strategy. In both the second and the fourth cutting stages, high fluctuations in the cutting force of CFRP/Ti6Al4V stacks are noted with the tool advancement due to the numerous brittle fractures in the chip separation of fibrous composites and the predominance of serrated chip formation for titanium alloys. The third stage denotes the complicated interface cutting featured by a rapid transition of the chip separation mode and a large variation of cutting forces in either the CFRP  $\rightarrow$  Ti or the Ti  $\rightarrow$  CFRP cutting sequence as

depicted in Fig. 3. The phenomena in some sense entail the instability of the tool-chip interaction and may excite tool chatter or even the premature failure of the inserts when the tool edge cuts across the interface region. It is also worth noting that the force profile of either CFRP phase or Ti phase gained in the post-cut process of a metallic-composite stack appears slightly higher than that generated in the initial-cut process of the stack, e.g., the  $F_c$  of the Ti phase in the CFRP  $\rightarrow$  Ti sequence is higher than that obtained in the Ti  $\rightarrow$  CFRP cutting sequence (Ref. Fig. 3). This is attributed to the effect of the chip adhesion arising from the initial-cut process on the subsequent cut process of the bi-material sandwich. The results are consistent with the findings of drilling CFRP/Ti6Al4V stacks subjected to different cutting sequences as reported by Xu and El Mansori [21].

The in-situ chip formation characteristics of CFRP/Ti6Al4V stacks were documented using a high-speed CCD camera with additional optical equipment necessary for obtaining a high-quality image. Figures 4, 5, and 6 show the typical frames gained during the orthogonal cutting tests with respect to different fiber orientations and cutting-sequence strategies under the identical cutting conditions of  $v_c = 80$  m/min and  $a_p = 0.20$  mm. The results presented in Fig. 4 indicate that when machining a 0° CFRP/Ti6Al4V stack under the CFRP  $\rightarrow$  Ti sequence, the tool edge cuts into the fibrous composite layer firstly and causes peel fracture initiating from the edge tip and propagating toward the fiber/matrix interface. With the tool advancement, the chip formation proceeds along the tool rake face until bending fracture occurs under cantilever loading, resulting in the dust-like chips spreading quickly into the surrounding environment as evidenced in Fig. 4a. The chip release for the 0° CFRP laminate is observed to be dominated by the fracture along the fiber/matrix interface and by the fracture perpendicular to the fiber axis under bending loads as stated by Wang et al. [23]. As the material removal occurs through numerous brittle fractures along the fiber/matrix interface with powdery chip formation, it accounts for the high-

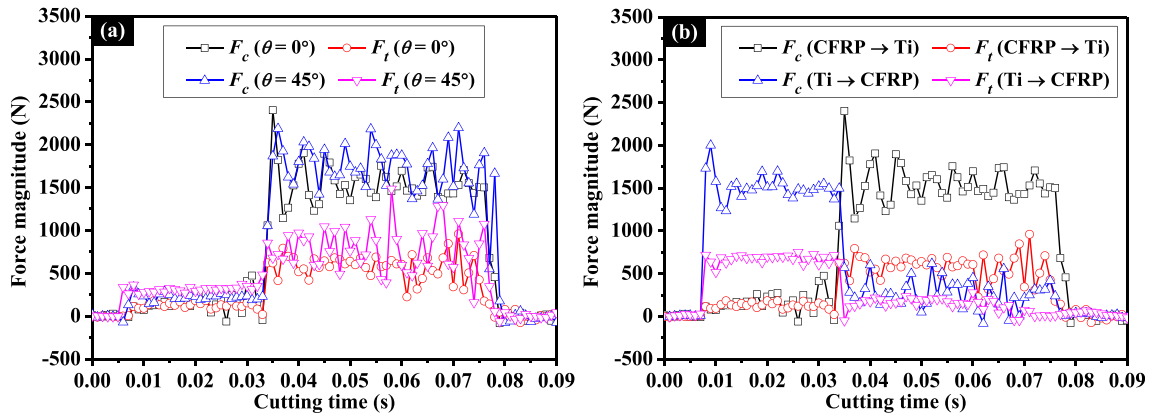
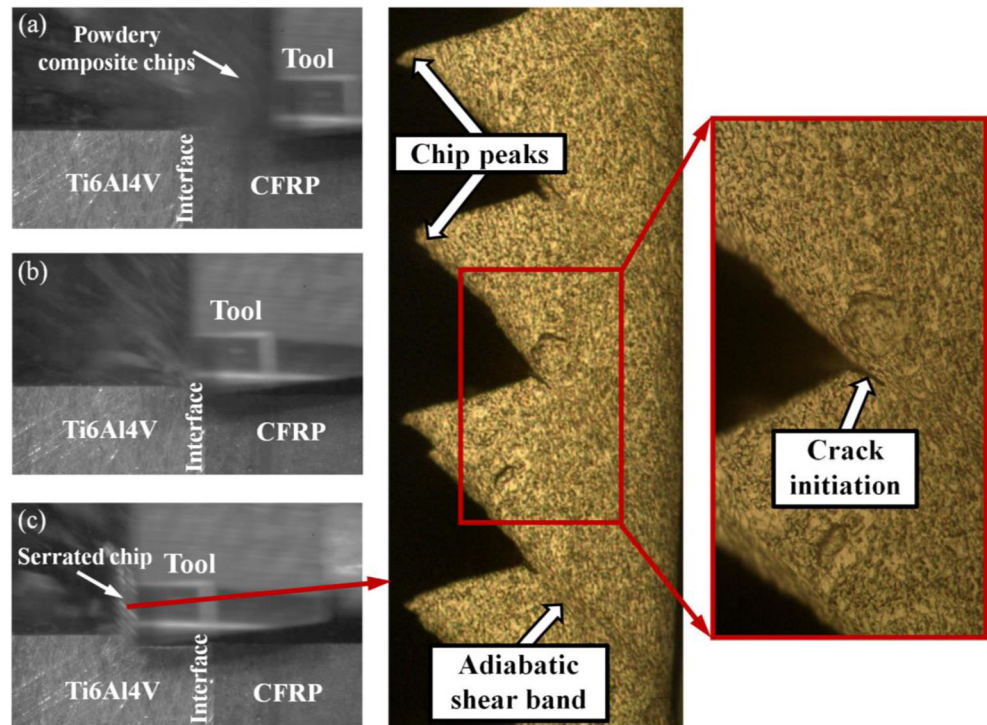


**Fig. 3** Evolution of force signals during the orthogonal cutting of CFRP/Ti6Al4V stacks ( $v_c = 80$  m/min and  $a_p = 0.20$  mm). **a** Force signatures with respect to different fiber orientations ( $\theta = 0^\circ$  and  $45^\circ$ ). **b**

Force signatures gained in cutting 0° CFRP/Ti6Al4V stacks subjected to different cutting sequences

**Fig. 4** High-speed camera images of the  $0^\circ$  CFRP/Ti6Al4V chip separation under the CFRP  $\rightarrow$  Ti cutting-sequence strategy ( $v_c = 80$  m/min and  $a_p = 0.20$  mm). **a** CFRP phase cutting. **b** Interface cutting. **c** Ti phase cutting



frequency fluctuations of cutting force signals as depicted in Fig. 3a. When the tool approaches the interface region, a rapid transition of the chip separation from brittle fracture to elastoplastic deformation takes place, leading to a dramatic increase of cutting forces as depicted in Fig. 3a. This phenomenon may initiate severe cutting vibrations as well as tool chatters during the stack cutting process, thus increasing the risk of catastrophic failure of tools like micro chipping or edge fracture. Owing to the rigid support provided by the adjacent Ti phase, the CFRP/Ti6Al4V interface zone is protected from damage, and neither interface delamination nor interlayer cracking is observed. As the tool attacks the titanium alloy, serrated but continuous chips are produced flowing along the tool rake face because of the elastoplastic behavior of the metallic phase. Large magnitudes of cutting forces and thrust forces are noted as well as high force fluctuations. The serrated chip formation for titanium alloys basically involves a two-stage process where the work material is plastically deformed ahead of the tool causing it to bulge. When a critical strain level is reached, catastrophic failure occurs, and a shear band is formed extending from the tool tip to the workpiece free surface. The resulting chips are composed of moderately formed chip segments separated by very narrow bands of highly sheared materials which are known as adiabatic shear bands. The adiabatic shear band is a form of failure mechanism and a precursor to ductile fracture occurring in the titanium chip removal process. As seen in Fig. 4, when machining titanium alloys at a cutting speed of 80 m/min, highly localized deformation zones and adiabatic shear bands are clearly visible through the metallographic examinations of

the chip cross section. In addition to the adiabatic shearing mechanism, micro cracks emanating from the chip free surface toward the primary shear zone are identified, operating as another key cause of serrated chip formation during the machining of the titanium phase.

Small discontinuous chips are initially noted when machining a  $45^\circ$  CFRP/Ti6Al4V stack under the CFRP  $\rightarrow$  Ti sequence (Ref. Fig. 5a) similar to those in cutting a  $0^\circ$  fiber-oriented stack. In cutting a positive fiber-oriented CFRP/Ti6Al4V stack (e.g.,  $\theta = 45^\circ$ ) the composite chip release occurs through the mechanisms of fracture resulting from the compression-induced shear across the fiber axis and the interfacial shearing along the fiber direction during the tool advancement which respectively refer to the primary fracture zone and the secondary fracture zone as denoted by Arola and Ramulu [28]. When the fracture reaches the composite free surface, it results in the complete chip formation at the macroscale. The material removal appears to be governed by in-plane shearing properties of the unidirectional laminate in the case of a positive fiber orientation. The post interface cutting and titanium cutting generally involve the identical chip removal process as discussed in the case of cutting the  $0^\circ$  CFRP/Ti6Al4V stack. When machining a higher fiber-oriented CFRP/Ti6Al4V (e.g.,  $\theta = 90^\circ$  or  $135^\circ$ ) (Ref. Fig. 5d–f and Fig. 5g–i), the CFRP chip separation becomes rather difficult due to the changes of the material removal process from in-plane shearing to out-of-plane fracture combined with severe macro deformation induced by the compressive tool load. The chips are basically generated in the form of discontinuous fiber bundles from a macroscale observation particularly for the cutting case of  $135^\circ$  CFRP/Ti6Al4V stacks.

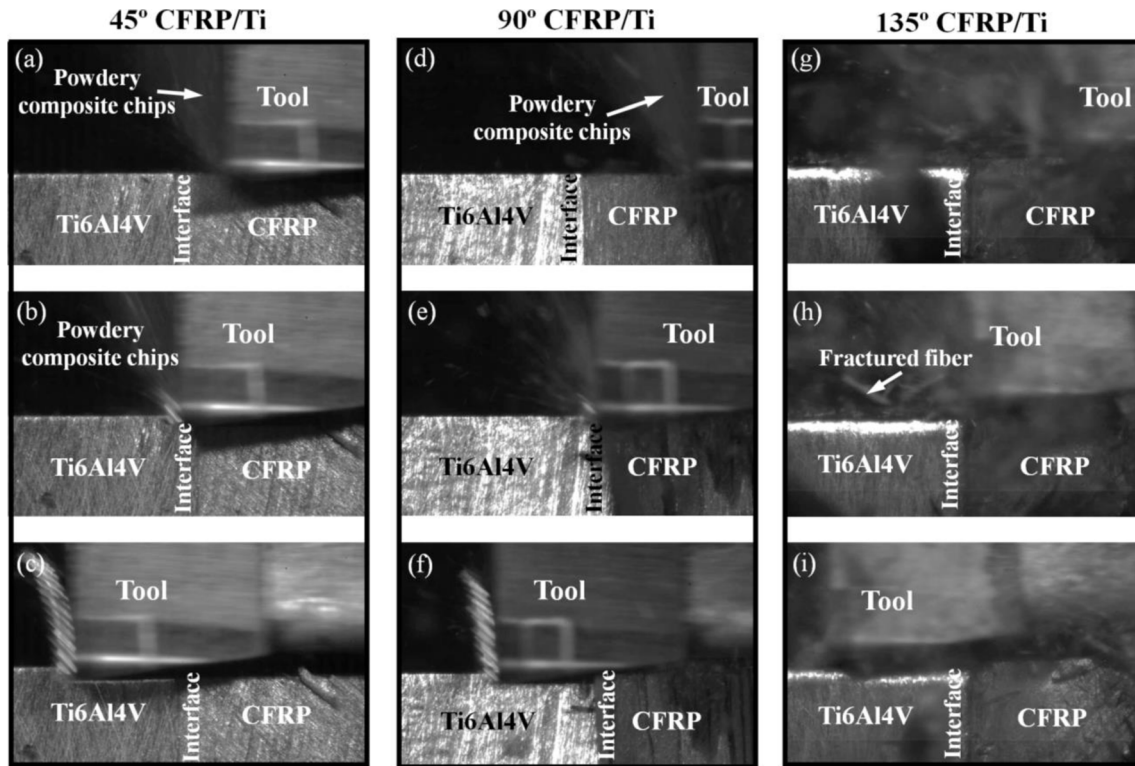


**Fig. 5** High-speed camera images of the CFRP/Ti6Al4V chip separation with respect to different fiber orientations under the CFRP  $\rightarrow$  Ti cutting-sequence strategy ( $v_c = 80$  m/min and  $a_p = 0.20$  mm). **a, d, g** CFRP phase cutting. **b, e, h** Interface cutting. **c, f, i** Ti phase cutting

A higher fiber orientation of the composite phase tends to result in more serious subsurface damage of the fiber/matrix system, which is evident by the highly visible interlaminar delamination of a cut  $90^\circ$  CFRP surface as exhibited in Fig. 5e. Besides, the cut carbon fibers existing on the composite surface under the compressive tool load would recover elastically and cause severe abrasions against the tool flank surface, contributing to the fluctuation of thrust forces. Additionally, when the tool cuts across the interface region, several discontinuous chips can adhere to the tool rake face and get wedged inside the tool/titanium chip interface, which may change the tool geometrical features and hence affect the resected titanium chip morphologies. The relevant results are discussed in subsection 3.3 - “Analysis of chips.”

On the contrary, the cutting characteristics for the Ti  $\rightarrow$  CFRP strategy appear to differ from those observed in the CFRP  $\rightarrow$  Ti cutting sequence. Similar to the findings of machining titanium alloys under the CFRP  $\rightarrow$  Ti sequence, the initial cut of the titanium alloy subjected to the utilized cutting conditions leads to the serrated chip formation regardless of the used fiber orientation. The elastoplastic deformation of the homogeneous metallic phase could promote highly localized temperatures at the tool-chip interface and give rise to hot and continuous chips. As the tool edge approaches the interface zone, the produced titanium chips become quite difficult to eject but stick onto the tool rake face that replace the

tool edge for the post-cut process of the interface region and CFRP phase as depicted in Fig. 6b, c. Afterward, the sharp-edged chip segments plow and rub against the uncut composite layer close to the stack interface, and the resulting cutting forces decrease quickly due to the rapid transition of the chip removal mode. In the interface machining of a  $45^\circ$  CFRP/Ti6Al4V stack, the cutting loads are uniquely applied on the uncut composite layer, and when the tensile stress of fibers at the interface vicinity exceeds the interface bonding strength, it results in a serious interlayer damage characterized by a V-shape-like morphology due to the poor rigidity provided by the adjacent composite layers. The Ti  $\rightarrow$  CFRP cutting is identified more liable to induce severe interface failure compared with the cutting from CFRP to Ti. As the tool is fully engaged in the cutting of the composite phase, the abrasion effects of the titanium chip adhesion on the CFRP surface tend to become more significant particularly when a higher fiber orientation is employed. This is evidenced by the fact that in machining a  $90^\circ$  CFRP/Ti6Al4V stack under the Ti  $\rightarrow$  CFRP sequence, the metallic chip adhesion causes a large extent of interlaminar cracking or delamination far beyond the cut surface (Ref. Fig. 6i), which severely deteriorates the cut stack surface quality and reduces its fatigue life for practical applications. Moreover, a detailed description of the key physical phenomena observed during the orthogonal



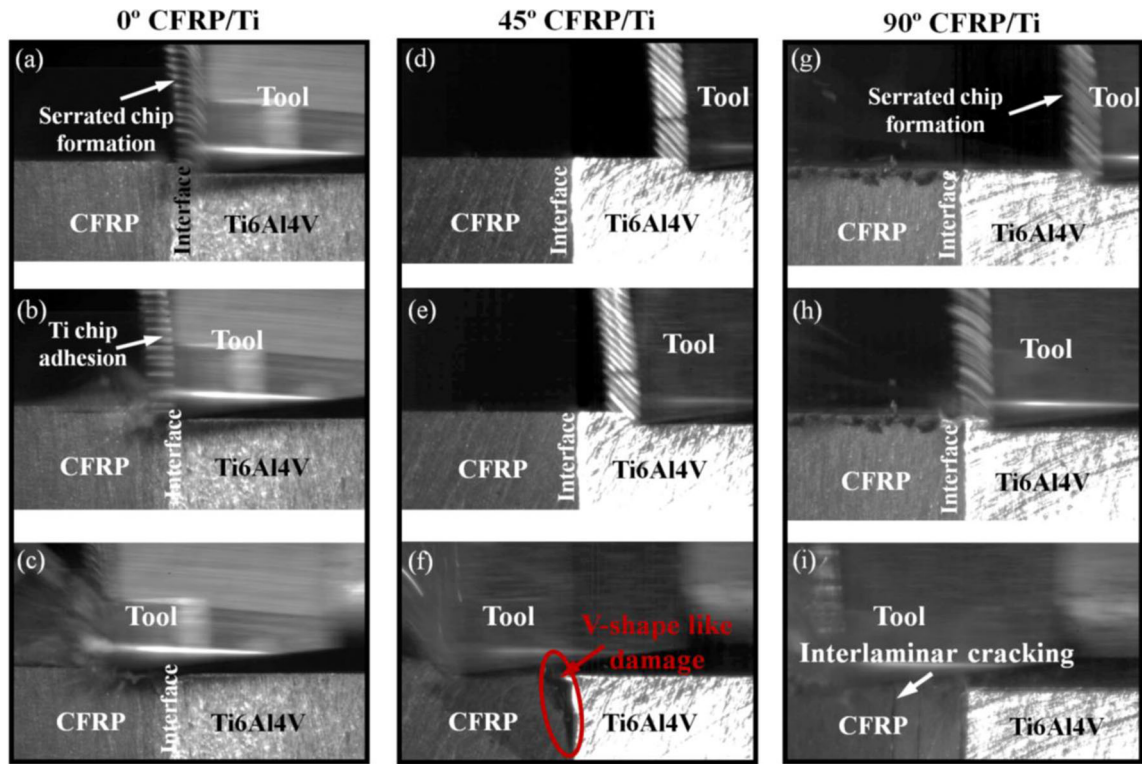


**Fig. 6** High-speed camera images of the CFRP/Ti6Al4V chip separation with respect to different fiber orientations under the Ti → CFRP cutting-sequence strategy ( $v_c = 80$  m/min and  $a_p = 0.20$  mm). **a, d, g** Ti phase cutting. **b, e, h** Interface cutting. **c, f, i** CFRP phase cutting

cutting of the stacks with respect to different cutting sequences is summarized in Table 2.

The in-situ chip removal analysis reveals the formation of discontinuous and serrated chips progressing along the tool rake face due to the predominance of brittle fracture and elastoplastic deformation in the stack machining. Both the fiber orientation and the cutting-sequence strategy affect greatly the chip separation process of the multilayer stacks. The chip release of the composite phase varies with the fiber orientation, which can be reflected in the signatures of cutting and thrust forces. Machining of the titanium phase is found to be governed by a mixture mode of thermoplastic instability of adiabatic shearing and the initiation/propagation of cracks in the primary shear zone, which results in the serrated chip formation. The cutting sequence plays a vital role in the material removal of the metallic-composite stacks mainly due to the influence arising from the chip adhesion on the post-cut process. Cutting from the composite phase to the metallic phase is found to facilitate an easy stack chip separation and hence guarantees excellent interface and composite surface quality.

### 3.2 Cutting forces and specific cutting energy

In orthogonal cutting of CFRP/Ti6Al4V stacks, the principle cutting force ( $F_c$ ) contributing to the chip separation process

was quantified versus different process parameters and cutting-sequence strategies. The cutting forces were measured at the steady cutting process for both the composite and metallic phases, and each measurement was repeated at least three times under the identical conditions so as to get reliable results. Fig. 7 shows the acquired force magnitudes of cutting 90° CFRP/Ti6Al4V stacks as a function of the cutting speed ( $v_c$ ) ( $a_p = 0.20$  mm) and depth of cut ( $a_p$ ) ( $v_c = 50$  m/min). It is noticeable that machining the titanium phase commonly produces much higher cutting forces approximately two or three times of those generated in the cutting of a 90° CFRP phase. The  $F_c$  magnitudes of the titanium phase basically decrease gradually with the cutting speed, which could be attributed to the softening effects of increased cutting temperatures on the titanium alloy when the cutting speed is elevated. By contrast, the cutting speed generally shows a minor but positive impact on the cutting forces of the CFRP phase as depicted in Fig. 7a. In addition, the  $F_c$  magnitudes of both the CFRP phase and Ti phase are found to show a linear proportion with the depth of cut during the cutting of CFRP/Ti6Al4V stacks regardless of the used cutting sequence. Moreover, the cutting-sequence strategy is confirmed to have a certain effect on the cutting force such that the post-cut process of a stacked phase often generates a higher  $F_c$  magnitude than the stacked phase being machined in an initial-cut process, which results from the influence of the chip adhesion during the stack cutting.

**Table 2** A summary of the key physical phenomena observed in the orthogonal cutting of CFRP/Ti6Al4V stacks

Cutting strategy	Fiber orientation ( $\theta$ )	Key phenomena observed in machining
CFRP $\rightarrow$ Ti	$\theta = 0^\circ$	(a) Initially, powdery chips rapidly spread to the surrounding environment being harmful to the respiratory systems of machinists. (b) Serrated Ti chips are produced on the tool rake face. (c) An amount of smoke is induced due to the high cutting heat produced in the Ti phase cutting. (d) Smooth interface and CFRP surfaces are generated.
	$\theta = 45^\circ$	(a) Initially, powdery chips rapidly spread to the surrounding environment being harmful to the respiratory systems of machinists. (b) Serrated Ti chips are generated flowing through the tool rake face. (c) An amount of smoke is induced due to the high cutting heat promoted in the Ti phase cutting. (d) Smooth interface and CFRP surfaces are produced.
	$\theta = 90^\circ$	(a) Difficult CFRP chip separation is observed due to the out-of-pane shear fracture along the fiber/matrix interface. (b) Quantities of discontinuous CFRP chips are formed. (c) Cracking damage propagates inside the CFRP laminate and interface zone. (d) Serrated Ti chips are produced on the tool rake face. (e) Poor CFRP and interface surfaces are generated.
Ti $\rightarrow$ CFRP	$\theta = 0^\circ$	(a) Initially, serrated Ti chips are produced accompanied by an amount of heat-induced smoke. (b) Ti chips tend to weld onto the tool rake face when the tool edge cuts into the interface zone. (c) Severe cracking takes place in the interface zone. (d) Finally, powdery CFRP chips are produced.
	$\theta = 45^\circ$	(a) Initially, serrated Ti chips are produced with an amount of heat-induced smoke. (b) Serious Ti chip adhesion is identified onto the tool rake face when the tool edge cuts into the interface zone. (c) "V-shape"-like delamination damage occurs in the interface zone. (d) Discontinuous CFRP chips are produced. (e) Poor CFRP and interface surfaces are generated.
	$\theta = 90^\circ$	(a) Initially, serrated Ti chips are produced accompanied by an amount of heat-induced smoke. (b) Serious Ti chip adhesion occurs on the tool rake face when the tool edge cuts into the interface zone. (c) Poor CFRP chip separation and difficult Ti chip ejection are observed. (d) Severe fiber/matrix splintering takes place within the CFRP laminate. (e) Extremely poor CFRP and interface surfaces are generated.

To evaluate the machinability of CFRP/Ti6Al4V stacks, the specific cutting energy ( $u - J/cm^3$ ) signifying the cutting energy consumed to remove one unit volume work material in the chip removal process was used for the assessment as defined below

$$u = \frac{P_c}{MMR} \quad (1)$$

where  $P_c$  denotes the machining power in  $W$  unit and  $MMR$  represents the material removal rate in  $cm^3/s$  unit.  $P_c$  and  $MMR$  can be further defined by

$$P_c = F_c \times v_c \quad (2)$$

$$MMR = v_c \times a_p \times a_w \quad (3)$$

where  $F_c$  signifies the main cutting force;  $v_c$  indicates the cutting speed;  $a_p$  and  $a_w$  denote the cutting depth and cutting width, respectively.

Then, the specific cutting energy ( $u$ ) can be expressed as follows [47]:

$$u = \frac{F_c}{a_p \times a_w} \quad (4)$$

The specific cutting energy ( $u$ ) is a characteristic parameter inherently determined by the mechanical properties of the used work-tool configuration. Figure 8 presents the  $u$

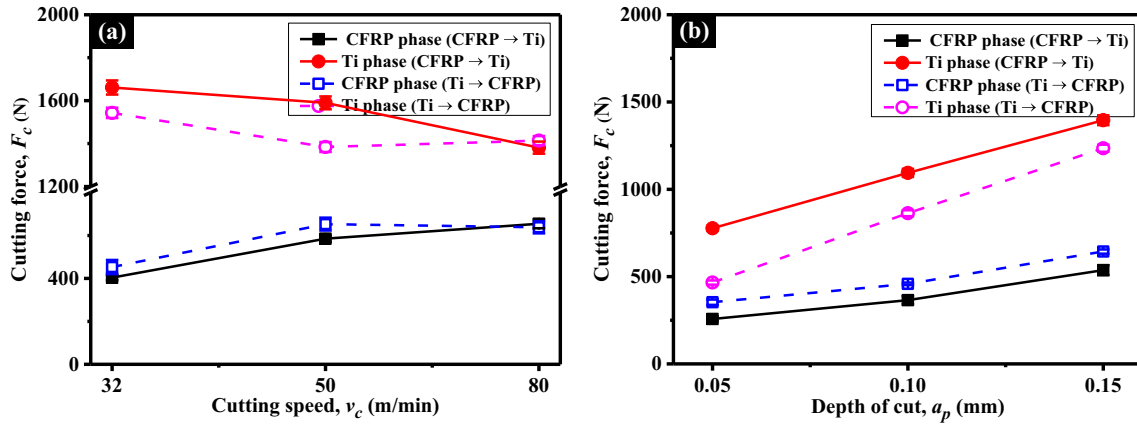


Fig. 7 Evolution of the cutting force ( $F_c$ ) with **a** the cutting speed ( $v_c$ ) ( $a_p = 0.20$  mm) and **b** the depth of cut ( $a_p$ ) ( $v_c = 50$  m/min) during the orthogonal cutting of 90° CFRP/Ti6Al4V stacks with respect to two different cutting-sequence strategies

values as a function of the cutting speed ( $v_c$ ) ( $a_p = 0.20$  mm) and the depth of cut ( $a_p$ ) ( $v_c = 50$  m/min) gained under the CFRP  $\rightarrow$  Ti cutting sequence, in which the  $u$  consumption was calculated separately based on each stacked phase machining. The results indicate that increasing the cutting speed ( $v_c$ ) tends to decrease the specific cutting energy consumption except the abnormal findings for the case of cutting a 90° CFRP phase as shown in Fig. 8a. The effects of the depth of cut on the specific cutting energy are totally negative for all examined fiber orientations such that an increased  $a_p$  leads to the decreased specific cutting energy and hence the improved machinability of the work material. Moreover, the Ti phase basically consumes more specific cutting energy than the CFRP phase regardless of the used cutting conditions. This is attributed to the homogeneous nature of the titanium alloy and its chip separation mode of elastoplastic deformation. Additionally, machining a higher fiber-oriented CFRP/Ti6Al4V stack basically consumes much more specific cutting energy compared with the cutting of CFRP/Ti6Al4V with a lower fiber orientation.

### 3.3 Analysis of chips

Chips produced in machining are key consequences depicting the characteristic details of the material removal, which offer an indirect observation of the underlying cutting mechanisms. As mentioned in subsection 3.1 - “Characteristics of CFRP/Ti6Al4V cutting process,” machining of CFRP/Ti6Al4V stacks involves two types of chip separation modes, resulting in the discontinuous and serrated chips. The resected CFRP chips are basically in the form of numerous tiny materials due to the predominance of brittle fracture mechanisms. The CFRP chip thickness was quantified based on the average measures of a set of chips gathered under a specific cutting condition via the help of SEM. Figure 9 presents the obtained thickness of the composite chips as a function of the fiber orientation ( $v_c = 50$  m/min and  $a_p = 0.20$  mm). It is worth noting that the chip thickness generally depicts a change with the fiber orientation. The phenomenon is attributed to the difference in chip separation mode as well as the associated fiber properties and interface behavior related

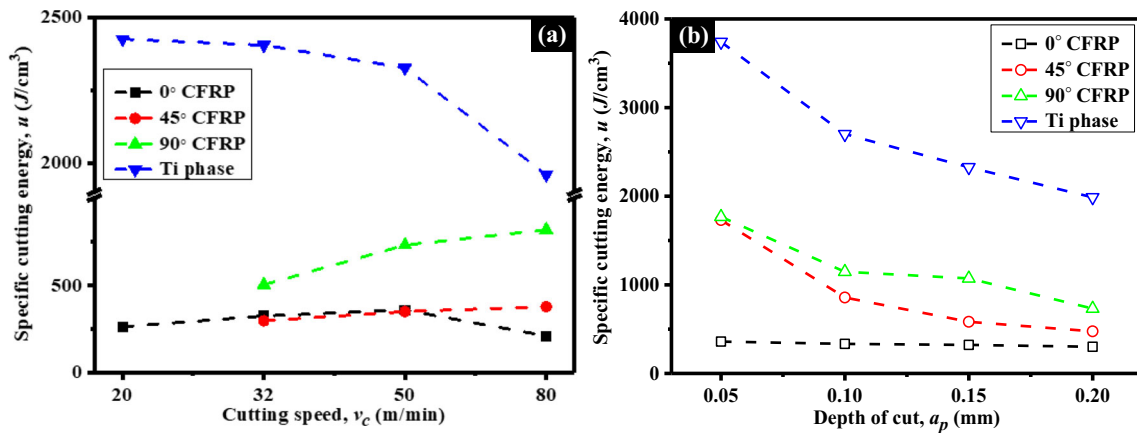


Fig. 8 Effects of **a** the cutting speed ( $v_c$ ) ( $a_p = 0.20$  mm) and **b** the depth of cut ( $a_p$ ) ( $v_c = 50$  m/min) on the specific cutting energy ( $u$ ) of CFRP/Ti6Al4V stacks under the CFRP  $\rightarrow$  Ti cutting sequence

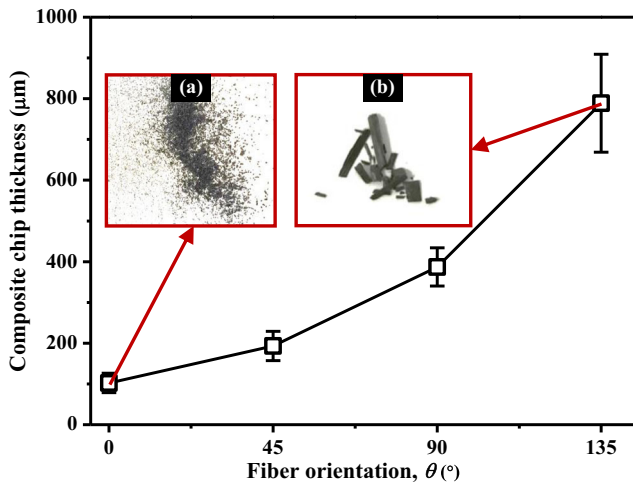


Fig. 9 Composite chip thickness as a function of fiber orientation in orthogonal cutting of CFRP/Ti6Al4V stacks ( $v_c = 50$  m/min and  $a_p = 0.20$  mm). **a**  $0^\circ$  CFRP chip morphology. **b**  $135^\circ$  CFRP chip morphology

inherently to the fiber orientation. As depicted in Fig. 9, when machining a  $0^\circ$  CFRP/Ti6Al4V stack, the resected composite chips appear quite powdery due to a series of fiber fractures occurring toward the tool cutting direction. On the contrary, the composite chips being generally in the form of bundles of fractured fibers with epoxy resin are noted when machining CFRP/Ti6Al4V stacks with a higher fiber orientation (e.g.,  $\theta = 135^\circ$ ) (Ref. Fig. 9b) since the chip separation is dominated by out-of-plane shear fracture along the fiber/matrix interface combined with severe macro deformation induced by the compressive tool load. In addition, since the cutting-sequence strategy was found to have a very negligible impact on the features of the composite chips, comparison of the CFRP chip thickness between two different cutting strategies was not provided in this paper.

Titanium chips generated from different cutting conditions were studied under both optical microscope and SEM to observe the overall pattern of segmentation and to characterize

their geometrical details. Figures 10 and 11 show the overall titanium chip shapes gained under different cutting speeds and depths of cut, respectively. The chips presented in the form of a microscopic examination were originally taken from the in-situ orthogonal cutting experiments without any post-process treatments to maintain their natural shapes after machining. Results indicate that even at a relatively low cutting speed (e.g.,  $v_c = 20$  m/min) Ti6Al4V still gives rise to serrated chip formation, and this segmentation phenomenon becomes more pronounced with increasing the cutting speed. Moreover, large depths of cut are more likely to induce visually apparent saw-tooth chips. On the other hand, the curling radius of the titanium chip is a characteristic parameter depending on the chip layer stiffness and tool geometries. This parameter in some sense implies the actual tool-chip contact length during titanium machining. The results given in Fig. 10 show that when machining CFRP/Ti6Al4V stacks at a constant depth of cut, the titanium chip curling radius basically remains unchanged regardless of the varying cutting speed. In contrast, it shows a high sensitivity to the depth of cut ( $a_p$ ) as depicted in Fig. 11 such that an increased  $a_p$  leads to an enlarged curling radius due to the increased stiffness of the chip layer.

Additionally, chip segmentation is a key characteristic when machining titanium alloys due to the thermoplastic instability and the initiation/propagation of cracks inside the primary shear zone. A schematic diagram of a typical serrated chip which outlines the general terminology used for quantitative analysis including chip peak ( $h_1$ ), chip valley ( $h_2$ ) and chip pitch ( $L_c$ ) is given in Fig. 12. The segmentation features of the titanium chips were quantified using an optical microscope according to the parameters defined in Fig. 12, and each measurement was repeated at least three times under the identical conditions in order to get reliable results. Figure 13 presents the titanium segmentation parameters gained from the CFRP  $\rightarrow$  Ti cutting sequence with respect to different fiber orientations under the fixed conditions of  $v_c = 50$  m/min and

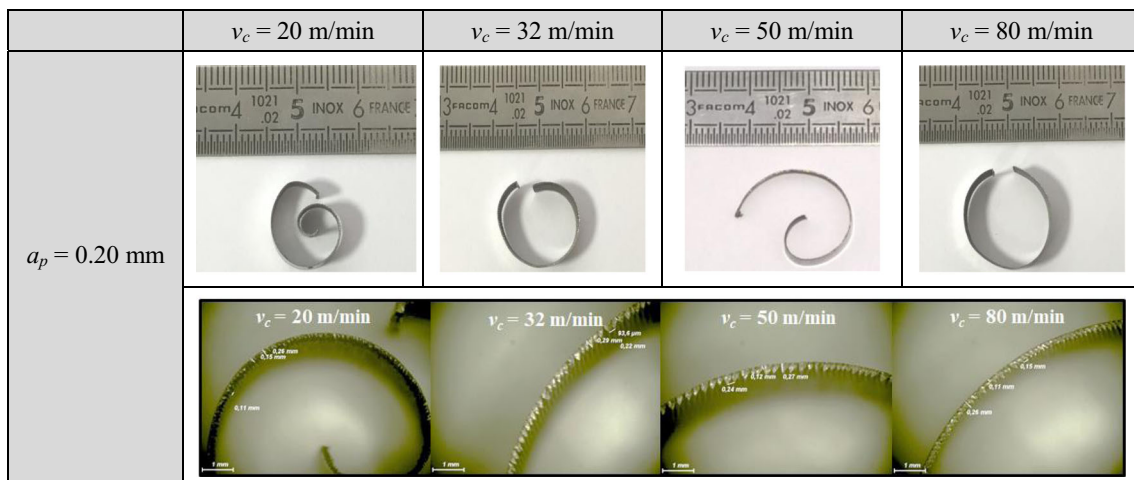


Fig. 10 Ti chip shapes gained under the CFRP  $\rightarrow$  Ti sequence with respect to different cutting speeds ( $v_c$ )

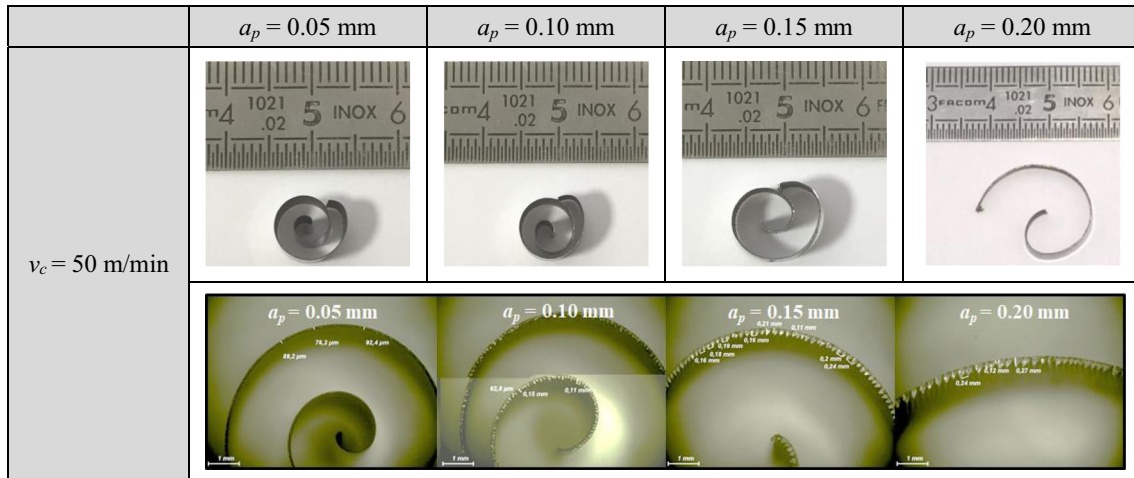


Fig. 11 Ti chip shapes gained under the CFRP → Ti sequence with respect to different depths of cut ( $a_p$ )

$a_p = 0.20$  mm. It is clear that machining CFRP phase firstly could affect the metallic chip geometries, which is evident by the variations of segmentation parameters in Fig. 13. The phenomenon is correlated with the geometrical modification of the tool edge and rake face resulting from the initial cut of the composite phase that changes the cutting conditions of the tool-chip interaction zone for the metallic phase.

Through the SEM examinations in Fig. 14, the back surface of the titanium chips defining the area in contact with the tool rake face appears very smooth and several adhered dust materials are identified which may be the composite debris resulting from the initial-cut process of the stack. The SEM images of the chip free surface show clearly the saw-tooth morphologies of titanium chips associated with regular chip peak, valley, and pitch obtained from different fiber-oriented CFRP/Ti6Al4V stacks. Moreover, the parametric effects on the titanium chip segmentation were studied in Fig. 15. The error bars in Fig. 15 denote the standard deviation of the

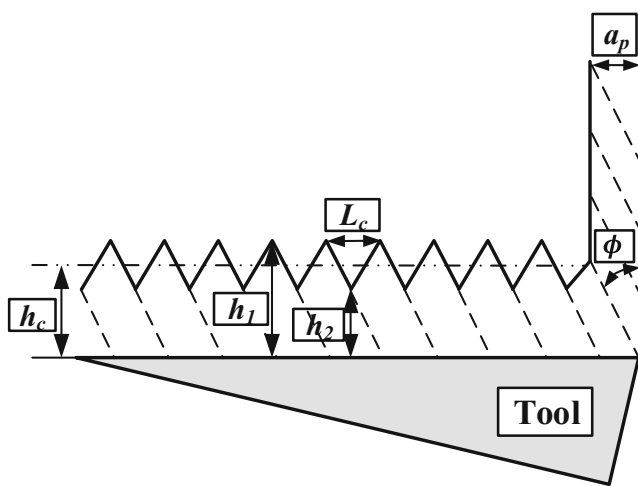
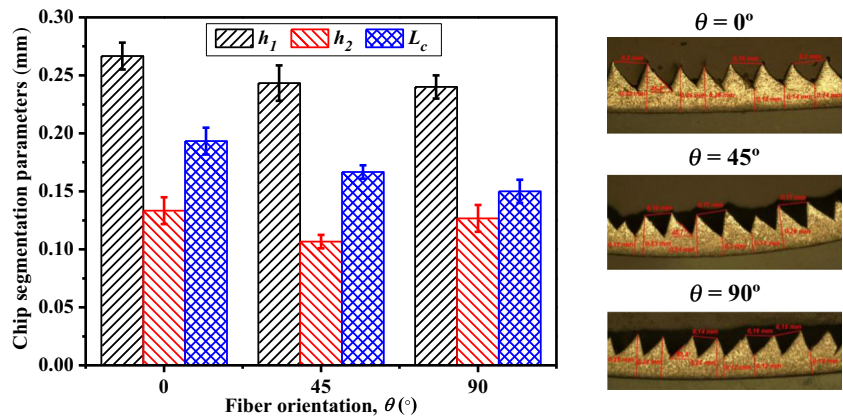


Fig. 12 A schematic illustration of definitions of the serrated chip geometries

dimensional magnitudes over the three measurement replications. To quantify the extent of the titanium chip segmentation, the  $S_i$  index defined as  $S_i = (h_1 - h_2)/h_1$  was introduced, and the results subjected to different cutting parameters are given in Fig. 16. Titanium chip segmentation as a result of a cycle of compression and adiabatic plastic shear process during the machining of CFRP/Ti6Al4V stacks is a key source responsible for the physical phenomena of high force fluctuations and cutting vibrations as well as tool chatter. The severe force fluctuation and tool chatter could result in dynamic stresses acting over a small tool-chip contact area, thus generating poor surface quality or initiating catastrophic tool failure like micro chipping or edge fracture. As such, the chip segmentation process of machining metallic-composite stacks needs to be effectively minimized in order to achieve better surface quality and longer tool life. In most cases, chip peaks and valleys determine the severity of chip serration while the chip pitch plays a vital role in the chip segmentation frequency. The cutting speed exhibits a negative impact on the chip peak and valley while it positively affects the chip pitch as seen in Fig. 15a. Both the chip peak and pitch increase linearly with the depth of cut as depicted in Fig. 15b. The enlarged chip pitch due to an elevated depth of cut basically implies the decreased segmentation frequency of the titanium chips. The findings are consistent with the observation of Cotterell and Byrne [48] in the orthogonal cutting of Ti6Al4V alloys. Further, the segmentation extent is identified susceptible to the cutting speed and depth of cut as shown in Fig. 16. The parametric effects on the  $S_i$  index are generally positive, which means that increasing either cutting speeds or depths of cut could accelerate the serration process of titanium chips during machining of CFRP/Ti6Al4V stacks. However, this situation is quite unfavorable for the minimization of cutting-induced vibrations and tool chatters, which may deteriorate the stack surface quality. The above analyses indicate the pivotal role of the fiber orientation in the composite chip shapes and the

**Fig. 13** Effects of the fiber orientation ( $\theta$ ) on the geometrical features of titanium chips ( $v_c = 50$  m/min and  $a_p = 0.20$  mm)



significant effects of the cutting speed and the depth of cut on the titanium chip segmentation.

### 3.4 Bouncing-back phenomenon

Bouncing back is a characteristic phenomenon widely observed during the machining of fibrous composites and related stacks but lacks quantitative analyses concerning its correlation with the input process parameters. This phenomenon happens when a part of the composite layer in the cutting path is pushed down during the chip removal process but springs back elastically after the tool passes away as stated by Wang and Zhang [26]. It is inherently associated with the elastic recovery of fibers undergoing deformation within the contact zone prior to fracture, and depends on the fiber stress status as well as the utilized fiber orientation. The bouncing-back phenomenon is generally considered detrimental to achieve high-quality machining of composites and related stacks, which is

attributed to its effects on rubbing against the tool flank surface causing abrasive wear, contributing to the thrust force generation and deteriorating the surface dimensional accuracy such as decreasing the hole diameter out of tolerance. The bouncing-back phenomenon during orthogonal cutting of CFRP/Ti6Al4V stacks was characterized using the difference between the nominal depth of cut and the real depth of cut. Figure 17 shows the results of the bouncing-back magnitudes against the variations of the fiber orientation and the nominal depth of cut under the CFRP  $\rightarrow$  Ti cutting sequence as well as several photographs of the cut CFRP surfaces under the fixed cutting speed of 50 m/min. Note that the magnitudes of the CFRP bouncing back correlate with the fiber orientation and the nominal depth of cut. In the case of machining a  $0^\circ$  CFRP/Ti6Al4V stack, the elastic recovery of cut fibers beneath the cutting plane may have a negligible effect on the measurements of the bouncing-back magnitude as the fiber orientation is perpendicular to the depth direction. Therefore,

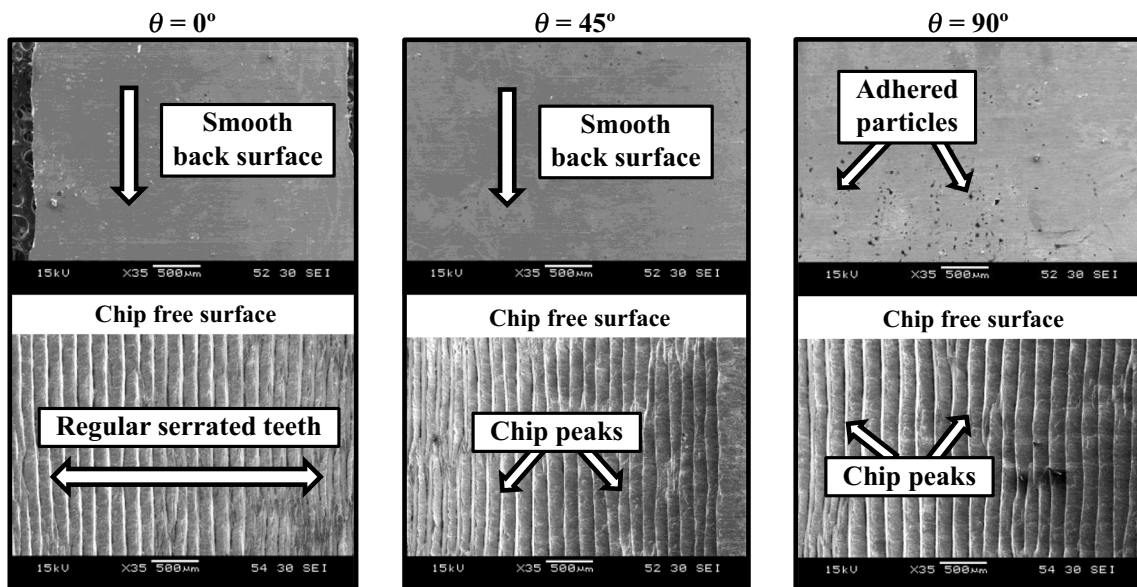


**Fig. 14** SEM micrographs of titanium chips showing the back surface and free surface formed in the CFRP  $\rightarrow$  Ti cutting sequence ( $v_c = 50$  m/min and  $a_p = 0.20$  mm)

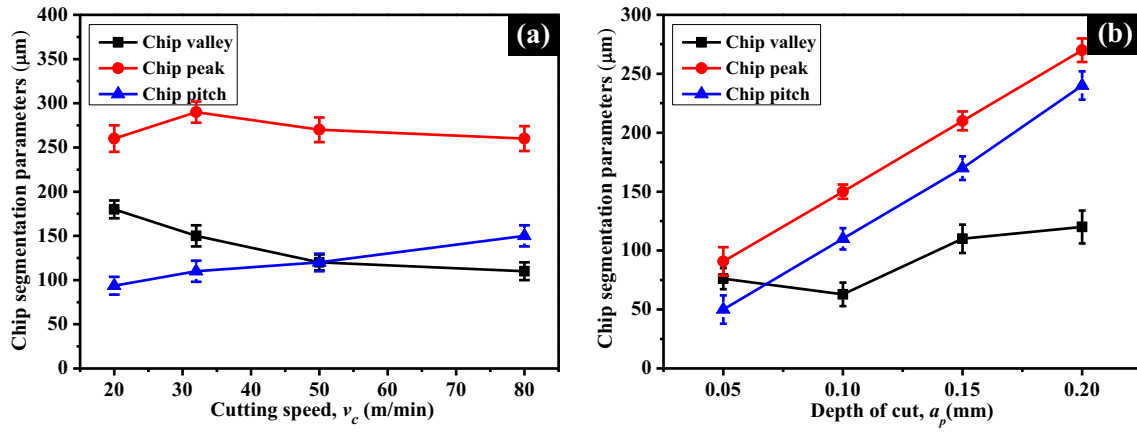


Fig. 15 Titanium chip segmentation parameters as a function of **a** cutting speed ( $v_c$ ) ( $a_p = 0.20$  mm) and **b** depth of cut ( $a_p$ ) ( $v_c = 50$  m/min)

the magnitudes of the bouncing back of the  $0^\circ$  CFRP/Ti6Al4V remain very low despite the varying nominal depth of cut. On the contrary, the CFRP bouncing back becomes more pronounced when the composite fiber orientation is greater than  $0^\circ$  (e.g.,  $\theta = 45^\circ$  and  $90^\circ$  in the present study) and its magnitude shows approximately a linearly increasing trend with the nominal depth of cut as evident in Fig. 17a. This can be explained by the fact that at a higher fiber orientation, many fibers are subjected to bending load but are not broken completely by the tool edge, resulting in a higher level of elastic recovery. Additionally, the serious defects of uncut fibers residing within the cut surface for a higher fiber-oriented CFRP/Ti6Al4V stack could increase the deviation of the CFRP bouncing-back magnitudes.

The relative significance of the composite bouncing back between different cutting sequences was examined with respect to the fiber orientation and the depth of cut. A comparative parameter defined by the difference between the bouncing-back magnitudes of two cutting strategies was

unitized to figure out which cutting sequence plays a more vital role in the composite bouncing back. The results given in Fig. 18 indicate an enhanced bouncing-back phenomenon of the stacked CFRP phase under the Ti  $\rightarrow$  CFRP cutting strategy, which is confirmed by a positive comparative magnitude for all examined cutting conditions. As discussed earlier, cutting from the metallic phase to the composite phase results in serious chip adhesion on the tool rake face that scratches and plows the uncut CFRP layers instead of shearing them. This causes a large number of incompletely cut fibers residing within the machined surface, which enhances the bouncing back of the composite phase. The phenomenon becomes much more significant particularly when a higher fiber orientation is applied as shown in Fig. 18. Moreover, increasing the nominal depth of cut is expected to enhance the relative predominance of the bouncing-back phenomenon under the Ti  $\rightarrow$  CFRP sequence. This agrees with the observation of the bouncing-back phenomenon occurring under the CFRP  $\rightarrow$  Ti strategy.

Fig. 16 Dependence of the chip segmentation index ( $S_i$ ) on the cutting parameters ( $v_c$  and  $a_p$ )

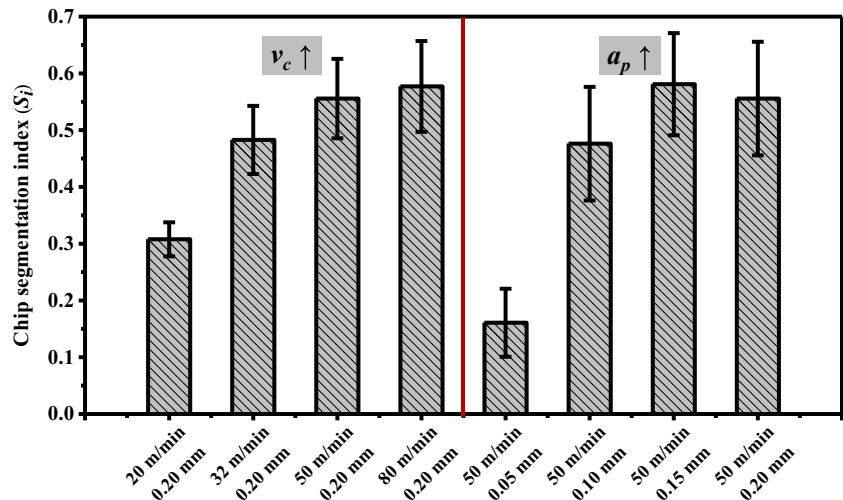
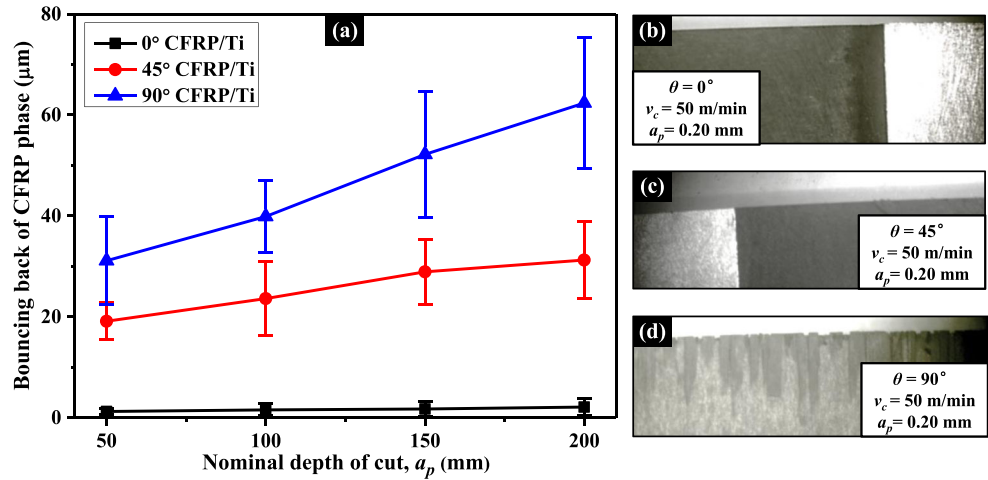


**Fig. 17** a Bouncing back of the CFRP phase gained under the CFRP → Ti cutting sequence ( $v_c = 50$  m/min) and optical photographs of b a cut  $0^\circ$  CFRP/Ti6Al4V, c a cut  $45^\circ$  CFRP/Ti6Al4V, and d a cut  $90^\circ$  CFRP/Ti6Al4V



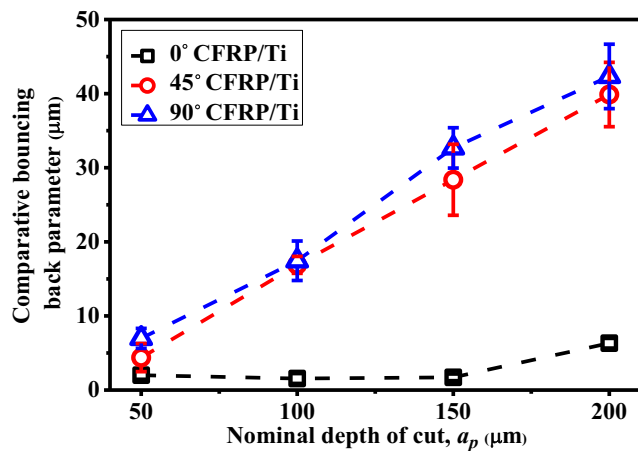
The above analyses indicate that the fiber orientation and the depth of cut both have a significantly positive impact on the bouncing-back phenomenon of the CFRP/Ti6Al4V stacks. The Ti → CFRP cutting sequence is confirmed to facilitate the stacked composite bouncing back, which may deteriorate the dimensional accuracy and surface quality of the cut stack. To ensure excellent stack surface quality, low fiber orientations, low depths of cut as well as a careful selection of the cutting strategy should be utilized for the multilayer stack machining.

### 3.5 Machined surface quality

The surface quality after cutting CFRP/Ti6Al4V stacks was examined using both an optical microscope and SEM. Figure 19 shows the overall morphologies of the machined stacks under the CFRP → Ti cutting strategy in terms of different fiber orientations. It is clear that the surface morphology of a machined metallic-composite stack is often fiber orientation dependent. Machining a lower fiber-oriented CFRP/Ti6Al4V stack generally gives rise to excellent surface finish without severe defects nor

failure. The cut metallic surface appears much flatter with minimal visual defects compared with the cut composite surface, which is attributed to the homogeneous nature of the titanium alloy as well as the chip removal mode of plastic deformation. The results in Fig. 19 a and b reveal the quite smooth surface morphologies of the machined  $0^\circ$  and  $45^\circ$  CFRP/Ti6Al4V stacks from a macroscopic observation. On the contrary, machining of CFRP/Ti6Al4V stacks with higher fiber orientations entails a rather difficult composite chip separation process, thus resulting in much poor surface morphologies as depicted in Fig. 19 c. In the case of a  $90^\circ$  CFRP/Ti6Al4V stack, the cut CFRP surface mainly consists of the finely cut composite surface distributed at the bottom region of the specimen and the defective surface characterized by numerous bare fibers residing particularly within the workpiece free edges along the cutting direction which are incompletely cut carbon fibers due to the severe out-of-plane shear fracture occurring with non-constraints of the workpiece edges.

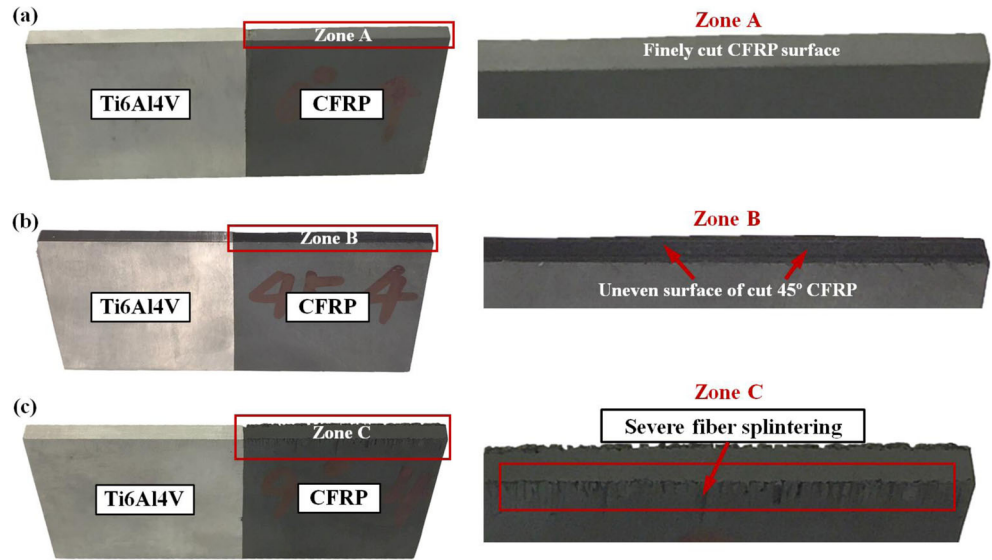
In addition to the optical inspections, microscopic examinations of the cut CFRP/Ti6Al4V surfaces with respect to different fiber orientations and cutting-sequence strategies were performed in order to identify the damage modes and the defect formation mechanisms of the multilayer material. Figure 20 shows the typical morphologies taken in the middle loci of the cut stack region after machining CFRP/Ti6Al4V stacks. It is found that the machined metallic surfaces appear much flatter and smoother in comparison with the interface and the composite surfaces as exhibited in Fig. 20. The cut CFRP surface morphologies are found highly dependent on the used fiber orientation, and the results of which are consistent with the optical observations presented in Fig. 19. Through the microscopic inspections, the damage morphologies of the low fiber-oriented CFRP surfaces (e.g.,  $\theta = 0^\circ$  and  $45^\circ$ ) are featured by short broken fibers covered by matrix smearing particularly in the center of the workpiece surface. Increasing the fiber orientation greatly deteriorates the machined composite surface morphologies and hence the surface

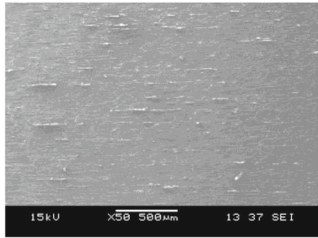
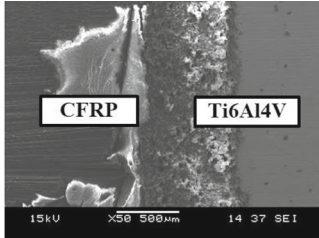
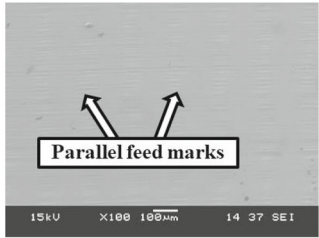
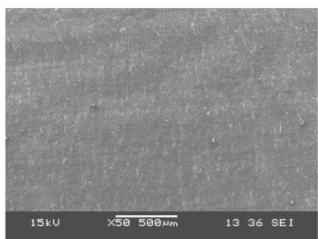
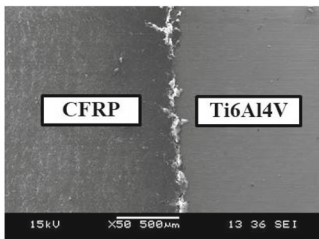
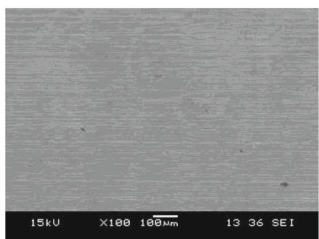
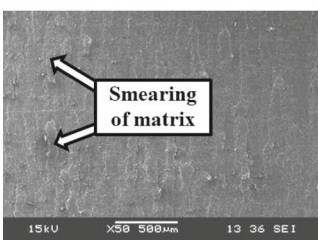
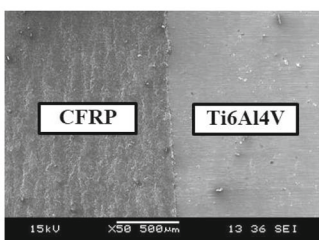
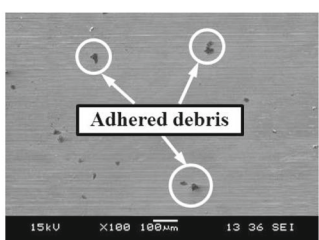
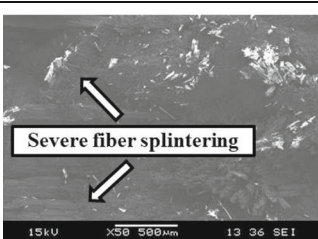
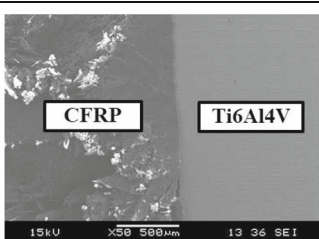
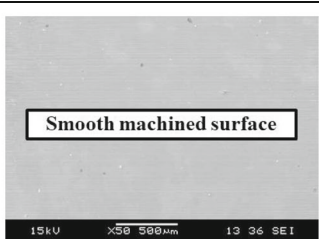


**Fig. 18** The relative significance of the CFRP bouncing back observed under different cutting-sequence strategies during the orthogonal cutting of CFRP/Ti6Al4V stacks ( $v_c = 50$  m/min)



**Fig. 19** Optical photographs showing the machined CFRP/Ti6Al4V stack surfaces under the CFRP → Ti sequence ( $v_c = 80$  m/min and  $a_p = 0.20$  mm). **a**  $\theta = 0^\circ$ . **b**  $\theta = 45^\circ$ . **c**  $\theta = 90^\circ$



	CFRP surface	Interface surface	Ti surface
$\theta = 0^\circ$			
$\theta = 45^\circ$			
$\theta = 90^\circ$			
$\theta = 135^\circ$			

**Fig. 20** SEM images of the machined CFRP/Ti6Al4V surface with respect to different fiber orientations. ( $v_c = 80$  m/min and  $a_p = 0.20$  mm)

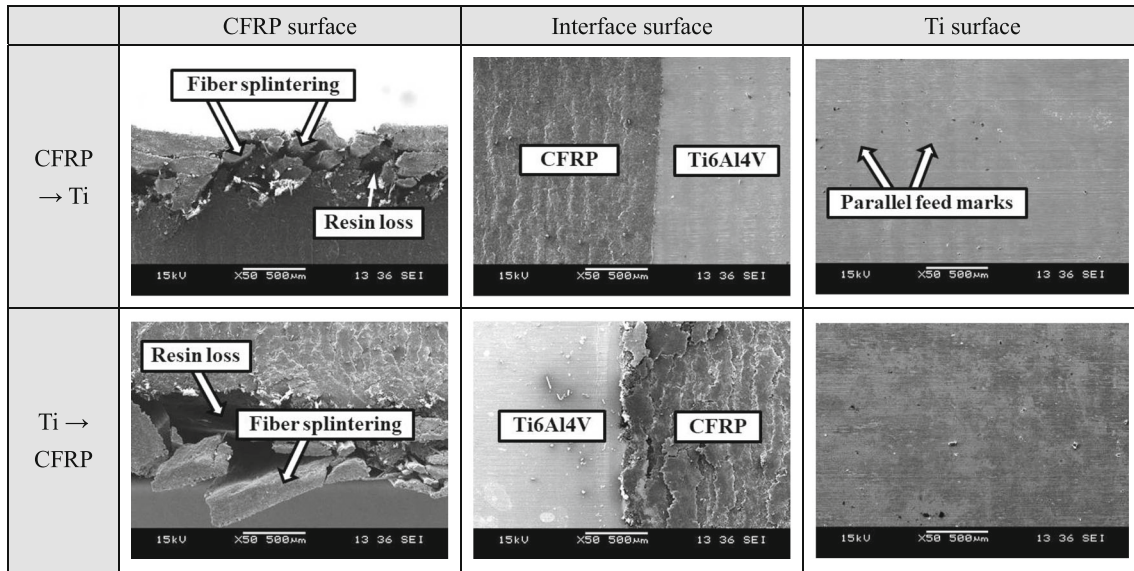


**Fig. 21** Comparative surface morphologies of 90° CFRP/Ti6Al4V stacks gained under two different cutting-sequence strategies ( $v_c = 50$  m/min and  $a_p = 0.20$  mm)

quality. The results in Fig. 20 show that when machining a 135° CFRP/Ti6Al4V stack, the composite surface is dominated by various fiber splintering due to the poor chip separation process associated with the out-of-plane shear fracture. By contrast, the titanium surfaces generated in the stack cutting consist of well-defined uniform feed marks running perpendicular to the tool cutting direction. The major surface defects observed include deformation of feed marks, micro-pits, and re-deposited debris onto the already machined titanium surface. The deformation of feed marks occurs mainly due to the plastic flow of the metallic phase in the cutting process, which may contribute to high surface roughness values as well as high residual stress levels. The micro-pit generation can be the results of brittle fractures of hard carbide inclusions within the immediate surface during the shearing of the workpiece by the tool. Additionally, the deposited particles onto the cut titanium surface may originate from the powdery composite chips

produced in the initial-cut process of the stack, which are detrimental to the functionality of the machined components. Physical damage like cracking is not identified on the titanium surface after the stack machining.

Figure 21 shows the comparative SEM morphologies of the machined 90° CFRP/Ti6Al4V surfaces under different cutting-sequence strategies ( $v_c = 50$  m/min and  $a_p = 0.20$  mm). It is clear that apart from the similar defects of the machined stack surface the cutting sequence indeed exhibits an impact on the quality of the CFRP surface and the interface region. Cutting from the composite to the metal generally promotes relatively minor defects or damage within the stack surface. The observed zone of the middle interface region could retain an intact and smooth surface even at the unfavorable 90° fiber orientation subjected to the CFRP → Ti cutting sequence. On the contrary, the Ti → CFRP cutting induces more serious fiber splintering and

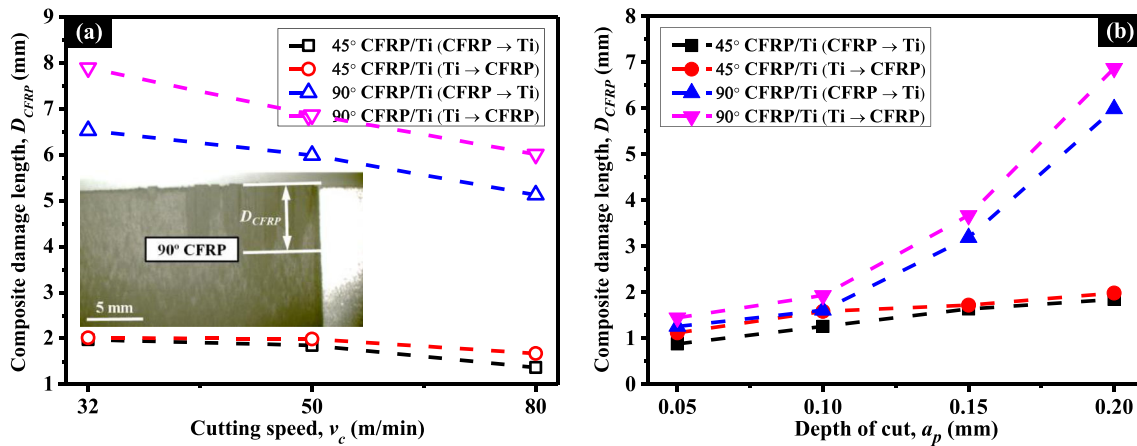


**Fig. 22** Composite damage length ( $D_{CFRP}$ ) of machined CFRP/Ti6Al4V stacks under different cutting sequences in terms of **a** cutting speed ( $a_p = 0.20$  mm) and **b** depth of cut ( $v_c = 50$  m/min)

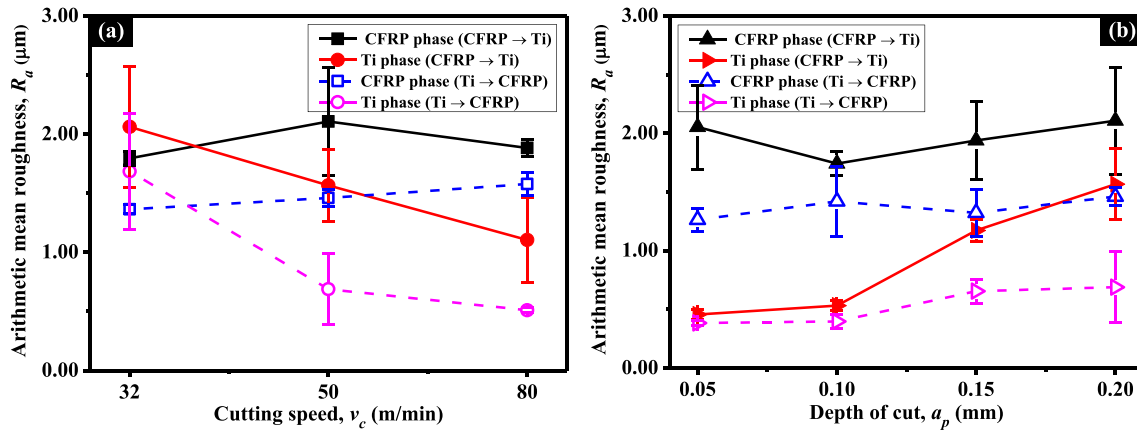


Fig. 23 Arithmetic mean roughness ( $R_a$ ) of machined  $0^\circ$  CFRP/Ti6Al4V stacks under different cutting sequences in terms of **a** cutting speed ( $a_p = 0.20$  mm) and **b** depth of cut ( $v_c = 50$  m/min)

fiber pullouts concentrated at the free edges of the composite surface as depicted in Fig. 21. The phenomenon is mainly due to the discrepancy in chip removal characteristics related to the cutting-sequence strategy.

Since the composite phase damage is the dominant defect during the machining of CFRP/Ti6Al4V stacks, the CFRP damage was quantified using the parameter ( $D_{CFRP}$ ) characterizing the maximum length from the cut surface to the deepest damaged zone. Figure 22 shows the calculated  $D_{CFRP}$  results after machining of CFRP/Ti6Al4V stacks with respect to different cutting conditions. Note that a higher fiber oriented stack is liable to induce a larger length of the composite-phase damage regardless of the used cutting speed or depth of cut. Machining from the composite phase to the metallic phase is confirmed favorable for the reduction of the  $D_{CFRP}$  due to the avoided influences resulting from the titanium cutting. On the other hand, the cutting speed and the depth of cut show the completely different impacts on the composite phase damage such that increasing the cutting speed tends to reduce the composite phase damage while an increase of the depth of cut will exacerbate the composite damage due to the elevated cutting forces (Ref. Figure 22). In general, the least CFRP damage can be achieved when high cutting speeds, low depths of cut as well as the CFRP  $\rightarrow$  Ti sequence are applied.

To evaluate the cut stack surface quality versus input process variables, the most-used surface roughness parameter—arithmetic mean roughness ( $R_a$ )—was adopted in the present study. Even though the  $R_a$  parameter cannot precisely depict the profile variations of a composite surface, it still represents the simplest method that could distinguish the parametric effects on the overall machined surface finish. Figure 23 presents the obtained results of machined  $0^\circ$  CFRP/Ti6Al4V stacks. It is clear that the  $R_a$  values of the cut titanium surfaces are always lower than those of the machined composite surfaces for all the cutting conditions investigated, which suggests a much better

surface finish of the metallic phase. Additionally, it is worth noting that both the cutting sequence and cutting parameters ( $v_c$  and  $f$ ) exhibit a similar impact on the surface roughness of the cut CFRP/Ti6Al4V stacks as they do on the composite-phase damage length ( $D_{CFRP}$ ). In general, the use of the highest cutting speed and the lowest depth of cut are found to favor the improvement of the cut stack quality. Such findings have also been seen in the machining of other metals and alloys as reported in the literature [49, 50].

## 4 Conclusions

This paper concerns an experimental investigation on the orthogonal cutting characteristics of CFRP/Ti6Al4V stacks using PCD-tipped tools. The orthogonal cutting mechanisms of the metallic-composite stacks including the chip removal process, cutting forces, chip features, bouncing-back phenomenon, and machined surface morphologies were carefully addressed with respect to the utilized process parameters. The impact of different cutting-sequence strategies on the CFRP/Ti6Al4V cutting response was clarified. The results of this investigation allow for a better comprehension of the complicated physical phenomena promoted in the multilayer stack machining. Based on the results acquired, the following conclusions are drawn.

- Machining of CFRP/Ti6Al4V stacks involves a combined material removal mechanism of brittle fracture and elastoplastic deformation, which leads to discontinuous and serrated chip formation. Both the fiber orientation and the cutting-sequence strategy are key factors greatly affecting the stack chip separation process. The chip release of the composite phase varies with the fiber orientation, which can be reflected in the signatures of cutting and thrust forces. The chip formation process of the titanium

alloy is found to be governed by a mixture mode of thermoplastic instability of adiabatic shearing and the initiation/propagation of cracks inside the primary shear zone. The stack interface represents the most difficult cutting zone which involves a rapid transition of chip separation mode leading to dramatic force variations, cutting vibrations, and tool chatter. The cutting sequence plays a vital role in the material removal of the metallic-composite stacks as a result of the influence from the chip adhesion on the post-cut process. The CFRP → Ti cutting is noted as a preferred strategy in favor of an easy chip separation that could guarantee excellent surface quality for CFRP/Ti6Al4V stacks.

- The principle cutting force accounting for the stack chip separation shows a high sensitivity to the cutting sequence as well as the cutting parameters. The cutting sequence has a certain impact on the cutting forces of CFRP/Ti6Al4V stacks such that the post-cut process of a stacked phase often generates a higher  $F_c$  magnitude than the identical stacked phase being machined in an initial-cut process. Increasing either the cutting speed or the depth of cut could lead to the decreased specific cutting energy consumption when machining CFRP/Ti6Al4V stacks. The fiber orientation is found to play a key role in the specific cutting energy consumption of the multilayer material. Cutting from the CFRP phase to the Ti phase is a reasonable strategy that could reduce both cutting forces and specific cutting energy consumption.
- The composite chip shapes released during machining of CFRP/Ti6Al4V stacks are highly dependent on the fiber orientation, and their thickness increases with the fiber orientation in the present investigation due to the change in chip separation associated with the fiber properties and fiber/matrix interface behavior relative to the cutting direction. The cutting-sequence strategy is observed to have a very negligible impact on the composite chip morphology. The titanium chip segmentation could be affected by the composite fiber orientation particularly subjected to the CFRP → Ti sequence. The cutting speed and depth of cut both affect significantly the geometrical features of the resected metallic chips as well as play a vital role in the chip segmentation extent.
- The bouncing-back phenomenon has been noted during the orthogonal cutting of CFRP/Ti6Al4V stacks, which correlates with the utilized depth of cut and the fiber orientation of the CFRP phase. The bouncing-back extent remains insignificant especially when machining a lower fiber-oriented CFRP/Ti6Al4V stack but becomes pronounced when higher fiber orientations and larger depths of cut are applied. Additionally, the Ti → CFRP cutting strategy is found capable of enhancing the severity of the composite bouncing back due to the titanium chip adhesion on the tool rake face that changes the cutting

conditions of the tool-chip interface. To guarantee accurate surface dimensions and good surface quality of cut metallic-composite stacks, low fiber orientations, low depths of cut as well as the CFRP → Ti cutting strategy should be utilized to reduce the bouncing-back effects.

- Defects of the cut CFRP/Ti6Al4V stacks mainly exist in the composite phase and the interface region. The cutting-induced composite damage manifests in the forms of fiber splintering, fiber pullouts, and matrix smearing while the main defect patterns for the cut titanium surfaces are featured by deformation of feed marks, micro-pits, and re-deposited particles onto the already machined titanium surface. The cutting-sequence strategy has a significant effect on the machined stack surface quality, and cutting from the composite to the metal favors the improvement of the machined surface finish. An increase in the cutting speed tends to decrease both the CFRP phase damage extent and the machined surface roughness while increasing the depth of cut shows an opposite impact. In the present study, the best surface finish of a cut CFRP/Ti6Al4V stack was achieved when the highest cutting speed, the lowest depth of cut as well as the CFRP → Ti cutting sequence were applied.

The analyses of the orthogonal cutting of CFRP/Ti6Al4V stacks in the present work could advance the state of knowledge of the subject area. A fundamental understanding on how the stack machinability is affected by the process parameters and the cutting sequences will lead to a reasonable strategy for high-quality machining of this multilayer material. Although the current studies were performed on a simplified orthogonal cutting process, the obtained knowledge can be applied to an actual stack drilling operation. Moreover, the present work can be further extended to combine with the numerical simulation technique to facilitate a more in-depth inspection of drilling CFRP/Ti6Al4V stacks.

**Funding information** The study was financially supported by the National Natural Science Foundation of China (Grant No.51705319), the Shanghai Pujiang Program (Grant No.17PJ1403800), and the Shanghai Academy of Spaceflight Technology (Grant No. SAST2017-060). The work was also partly sponsored by the Research Project of State Key Laboratory of Mechanical System and Vibration (Grant No. MSVZD201704).

## References

1. SenthilKumar M, Prabukarhi A, Krishnaraj V (2013) Study on tool wear and chip formation during drilling carbon fiber reinforced polymer (CFRP)/titanium alloy (Ti6Al4V) stacks. *Procedia Eng* 64:582–592

2. Pecat O, Brinksmeier E (2014) Tool wear analyses in low frequency vibration assisted drilling of CFRP/Ti6Al4V stack material. *Procedia CIRP* 14:142–147
3. Xu J, El Mansori M (2017) Wear characteristics of polycrystalline diamond tools in orthogonal cutting of CFRP/Ti stacks. *Wear* 376-377:91–106
4. Xu J, Mkkaddem A, El Mansori M (2016) Recent advances in drilling hybrid FRP/Ti composite: a state-of-the-art review. *Compos Struct* 135:316–338
5. Tsao CC (2008) Experimental study of drilling composite materials with step-core drill. *Mater Des* 29(9):1740–1744
6. Sorrentino L, Turchetta S, Bellini C (2017) In process monitoring of cutting temperature during the drilling of FRP laminate. *Compos Struct* 168:549–561
7. Sorrentino L, Turchetta S, Bellini C (2018) A new method to reduce delaminations during drilling of FRP laminates by feed rate control. *Compos Struct* 186:154–164
8. Abhishek K, Datta S, Mahapatra SS (2014) Optimization of thrust, torque, entry, and exist delamination factor during drilling of CFRP composites. *Int J Adv Manuf Technol* 76(1–4):401–416
9. Tsao CC, Kuo KL, Hsu IC (2012) Evaluation of a novel approach to a delamination factor after drilling composite laminates using a core-saw drill. *Int J Adv Manuf Technol* 59(5):617–622
10. Ramulu M, Branson T, Kim D (2001) A study on the drilling of composite and titanium stacks. *Compos Struct* 54(1):67–77
11. Brinksmeier E, Janssen R (2002) Drilling of multi-layer composite materials consisting of carbon fiber reinforced plastics (CFRP), titanium and aluminum alloys. *CIRP Ann Manuf Technol* 51(1):87–90
12. Krishnaraj V, Zitoune R, Collombet F (2010) Comprehensive review on drilling of multimaterials stacks. *J Mach Form Technol* 2(3–4):1–32
13. Park KH, Beal A, Kim D, Kwon P, Lantrip J (2011) Tool wear in drilling of composite/titanium stacks using carbide and polycrystalline diamond tools. *Wear* 271(11–12):2826–2835
14. Tashiro T, Fujiwara J, Inada K (2011) Drilling of CFRP/Ti-6Al-4V stacks. *Adv Mater Res* 325:369–374
15. Isbilir O, Ghassemieh E (2013) Comparative study of tool life and hole quality in drilling of CFRP/titanium stack using coated carbide drill. *Mach Sci Technol* 17(3):380–409
16. Wang X, Kwon PY, Sturtevant C, Kim D, Lantrip J (2014) Comparative tool wear study based on drilling experiments on CFRP/Ti stack and its individual layers. *Wear* 317(1–2):265–276
17. Sanda A, Arriola I, Navas VG, Bengoetxea I, Gonzalo O (2016) Ultrasonically assisted drilling of carbon fibre reinforced plastics and Ti6Al4V. *J Manuf Process* 22:169–176
18. Zhang L, Liu Z, Tian W, Liao W (2015) Experimental studies on the performance of different structure tools in drilling CFRP/Al alloy stacks. *Int J Adv Manuf Technol* 81(1–4):241–251
19. Alberdi A, Artaza T, Suárez A, Rivero A, Girot F (2015) An experimental study on abrasive waterjet cutting of CFRP/Ti6Al4V stacks for drilling operations. *Int J Adv Manuf Technol*: 1–14
20. Wang H, Qin X, Li H, Tan Y (2016) A comparative study on helical milling of CFRP/Ti stacks and its individual layers. *Int J Adv Manuf Technol* 86(5):1973–1983
21. Xu J, El Mansori M (2016) Experimental study on drilling mechanisms and strategies of hybrid CFRP/Ti stacks. *Compos Struct* 157: 461–482
22. Koplev A, Lystrup A, Vorm T (1983) The cutting process, chips, and cutting forces in machining CFRP. *Compos* 14(4):371–376
23. Wang DH, Ramulu M, Arola D (1995) Orthogonal cutting mechanisms of graphite/epoxy composite. Part I: unidirectional laminate. *Int J Mach Tools Manuf* 35(12):1623–1638
24. Arola D, Ramulu M, Wang DH (1996) Chip formation in orthogonal trimming of graphite/epoxy composite. *Compos Pt A - Appl Sci Manuf* 27(2):121–133
25. Pwu H, Hocheng H (1998) Chip formation model of cutting fiber-reinforced plastics perpendicular to fiber axis. *J Manuf Sci Eng-Trans ASME* 120(1):192–196
26. Wang XM, Zhang LC (2003) An experimental investigation into the orthogonal cutting of unidirectional fibre reinforced plastics. *Int J Mach Tools Manuf* 43(10):1015–1022
27. Brinksmeier E, Fangmann S, Rentsch R (2011) Drilling of composites and resulting surface integrity. *CIRP Ann Manuf Technol* 60(1): 57–60
28. Arola D, Ramulu M (1997) Orthogonal cutting of fiber-reinforced composites: a finite element analysis. *Int J Mech Sci* 39(5):597–613
29. Arola D, Sultan MB, Ramulu M (2002) Finite element modeling of edge trimming fiber reinforced plastics. *J Manuf Sci Eng-Trans ASME* 124(1):32–41
30. Nayak D, Bhatnagar N, Mahajan P (2005) Machining studies of UD-FRP composites part 2: finite element analysis. *Mach Sci Technol* 9(4):503–528
31. Venu Gopala Rao G, Mahajan P, Bhatnagar N (2007) Micro-mechanical modeling of machining of FRP composites - cutting force analysis. *Compos Sci Technol* 67(3–4):579–593
32. Lasri L, Nouari M, El Mansori M (2009) Modelling of chip separation in machining unidirectional FRP composites by stiffness degradation concept. *Compos Sci Technol* 69(5):684–692
33. Iliescu D, Gehin D, Iordanoff I, Girot F, Gutiérrez ME (2010) A discrete element method for the simulation of CFRP cutting. *Compos Sci Technol* 70(1):73–80
34. Calamaz M, Coupard D, Girot F (2008) A new material model for 2D numerical simulation of serrated chip formation when machining titanium alloy Ti-6Al-4V. *Int J Mach Tools Manuf* 48(3–4): 275–288
35. Nurul Amin AKM, Ismail AF, Nor Khairushima MK (2007) Effectiveness of uncoated WC-Co and PCD inserts in end milling of titanium alloy—Ti-6Al-4V. *J Mater Process Technol* 192:147–158
36. Komanduri R, Von Turkovich BF (1981) New observations on the mechanism of chip formation when machining titanium alloys. *Wear* 69(2):179–188
37. Komanduri R, Hou ZB (2002) On thermoplastic shear instability in the machining of a titanium alloy (Ti-6Al-4V). *Metall Mater Trans A* 33(9):2995–3010
38. Molinari A, Musquar C, Sutter G (2002) Adiabatic shear banding in high speed machining of Ti-6Al-4V: experiments and modeling. *Int J Plasticity* 18(4):443–459
39. Vyas A, Shaw MC (1999) Mechanics of saw-tooth chip formation in metal cutting. *J Manuf Sci Eng-Trans ASME* 121(2):163–172
40. Hua J, Shivpuri R (2004) Prediction of chip morphology and segmentation during the machining of titanium alloys. *J Mater Process Technol* 150(1–2):124–133
41. Poutord A, Rossi F, Poulachon G, M'Saoubi R, Abrivard G (2013) Local approach of wear in drilling Ti6Al4V/CFRP for stack modelling. *Procedia CIRP* 8:316–321
42. Xu J, El Mansori M, Voisin J (2016) Numerical modeling and FE analysis of CFRP/Ti stack orthogonal cutting. *Procedia CIRP* 46(1): 67–70
43. Xu J, El Mansori M (2016) Numerical modeling of stacked composite CFRP/Ti machining under different cutting sequence strategies. *Int J Precis Eng Manuf* 17(1):99–107
44. Xu J, El Mansori M (2016) Numerical studies of frictional responses when cutting hybrid CFRP/Ti composite. *Int J Adv Manuf Technol* 87(1):657–675
45. Xu J, El Mansori M (2016) Experimental studies on the cutting characteristics of hybrid CFRP/Ti stacks. *Procedia Manuf* 5:270–281
46. Xu J, El Mansori M (2016) An experimental investigation on orthogonal cutting of hybrid CFRP/Ti stacks. *AIP Conference Proceedings* 1769(1):080002

47. Shaw MC (2005) Metal cutting principles. 2nd edn. Oxford University Press, New York
48. Cotterell M, Byrne G (2008) Dynamics of chip formation during orthogonal cutting of titanium alloy Ti-6Al-4V. *CIRP Ann Manuf Technol* 57(1):93–96
49. Yousuff CM, Danish M, Ho ETW, Kamal Basha IH, Hamid NHB (2017) Study on the optimum cutting parameters of an aluminum mold for effective bonding strength of a PDMS microfluidic device. *Micromachines* 8(8):258
50. Danish M, Ginta TL, Habib K, Carou D, Rani AMA, Saha BB (2017) Thermal analysis during turning of AZ31 magnesium alloy under dry and cryogenic conditions. *Int J Adv Manuf Technol* 91(5):2855–2868

**Publisher's note** Springer Nature remains neutral with regard to jurisdictional claims in published maps and institutional affiliations.